Check for updates

Received: 21 August 2025 | Revised: 6 March 2026 | Accepted: 18 March 2026

DOI: 10.1002/dep2.70071

The Depositional Record
A journal of the International Association of Sedimentologists
Open Access
IAS
WILEY

ORIGINAL ARTICLE

The Permian–Triassic transition in Türkiye: New insights and 3D outcrop models for accessible, reproducible and sustainable fieldwork

Baran Karapunar[1] | **Xia Wang**[2] | **Stella Z. Buchwald**[3] | **Anja B. Frank**[3] | **Mónica Alejandra Gómez Correa**[3] | **Müjde Gürsoy**[4] | **Zhipeng Liu**[5] | **Xuanni Xu**[2] | **Lingzan Meng**[2] | **Damla Demir**[6] | **Erdal Koşun**[7] | **Aymon Baud**[8] | **William J. Foster**[3]

[1]School of Earth and Environment, University of Leeds, Leeds, UK

[2]Key Laboratory of Deep-time Geography and Environment Reconstruction and Application of Ministry of Natural Resources, Institute of Sedimentary Geology, Chengdu University of Technology, Chengdu, China

[3]Department of Earth System Sciences, Institute for Geology, University of Hamburg, Hamburg, Germany

[4]MTA Şehit Cuma Dağ Natural History Museum, General Directorate of Mineral Research and Exploration, Çankaya, Ankara, Türkiye

[5]College of Geophysics, Chengdu University of Technology, Chengdu, China

[6]Department of Geological Engineering, Kütahya Dumlupınar University, Kütahya, Türkiye

[7]Department of Geological Engineering, Akdeniz University, Antalya, Türkiye

[8]Institute of Earth Sciences, Geopolis, University of Lausanne, Lausanne, Switzerland

Correspondence
Baran Karapunar, School of Earth and Environment, University of Leeds, Leeds LS2 9JT, UK.
Email: b.karapunar@leeds.ac.uk

Xia Wang, Key Laboratory of Deep-time Geography and Environment Reconstruction and Application of Ministry of Natural Resources, Institute of Sedimentary Geology, Chengdu University of Technology, Chengdu 610059, China.
Email: xiawang@cdut.edu.cn

Funding information
Deutsche Forschungsgemeinschaft, Grant/Award Number: FO1297/1-1; Natural Environment Research Council, Grant/Award Number: NE/X012859/1 and NE/X015025/1; MTA General Directorate of Mineral Research and Exploration, Grant/Award Number: 2024-08-16-02-1; The National Natural Science Foundation of

Abstract

The Permian–Triassic transition is characterised by major environmental changes and the largest known mass extinction event in the Phanerozoic. However, successions with a relatively complete sedimentological and palaeontological record across the Permian–Triassic are limited to a few well-known sections. The Antalya and Aladağ Nappes in south-western Türkiye provide extensive outcrops of the Permian–Triassic transition. Some key investigations have revealed the importance and potential for these successions to improve our understanding of the events across the Permian–Triassic. Here, we incorporate 3D open-access virtual outcrop models with a virtual field guide to introduce the Permian–Triassic transition in south-western Türkiye, to improve the accessibility, reproducibility and sustainability of fieldwork findings. The fossiliferous Upper Permian to Lower Triassic successions in the studied locations reach over a kilometre thickness. Due to the contemporaneous opening of the Neotethys Ocean, the exposures from the Antalya Nappe (Çürük Dağ in Kemer; Öznurtepe in Gazipaşa; and Demirtaş in Alanya) are considered to be deposited on a southward facing carbonate platform in the Neotethys Ocean, whilst successions from the Aladağ Nappe (Taşkent

This is an open access article under the terms of the Creative Commons Attribution License, which permits use, distribution and reproduction in any medium, provided the original work is properly cited.
© 2026 The Author(s). *The Depositional Record* published by John Wiley & Sons Ltd on behalf of International Association of Sedimentologists.

China (NSFC), Grant/Award Number: 42293291 and 42102143

in Konya) are considered to be deposited on the northern side of the carbonate platform towards the Palaeotethys Ocean. In all sections, the Changhsingian (uppermost Permian) is represented by highly fossiliferous platform carbonates. The Changhsingian successions terminate with a thin oolitic grainstone ('transitional oolites'), which is identified as the Permian–Triassic mass extinction interval and is characterised by a negative carbon isotope excursion. The transitional oolites are overlain by microbialite-dominated carbonates, and then oolite-dominated carbonates deposited in the Griesbachian. This carbonate-rich deposition was replaced with a mixed carbonate-siliciclastic succession later in the Early Triassic (Dienerian–Spathian), when marine ecosystems slowly recovered. These environmental and biotic changes are similar to the known record from the tropical palaeolatitudes in the western to eastern Palaeotethys.

KEYWORDS

FAIR principles, mass extinction, Permian, Triassic, Turkey, virtual outcrop models

1 | INTRODUCTION

The Permian–Triassic transition records the largest known mass extinction event in Earth's history (Marshall, 2023). Extreme environmental changes, such as climate warming at a rapid pace and high magnitude (Gliwa et al., 2022), ocean acidification (Jurikova et al., 2020) and expansion of ocean deoxygenation (Sperling et al., 2022), driven by carbon dioxide emissions associated with the eruptions of the Siberian Traps Large Igneous Province and arc volcanism are postulated as the extinction drivers (e.g. Dal Corso et al., 2022; Zhang et al., 2021). This renders the event important for understanding the co-evolution of life and the planet in extreme conditions, whilst also potentially offering insights into projected environmental and ecological perturbations. However, what is known about the Permian–Triassic transition is heavily biased by well-studied sections in South China, because those sections have a well-constrained stratigraphic framework allowing for high resolution investigations (e.g. Shen et al., 2011; Wang et al., 2014). There are other well-studied regions around the world that are key for understanding this event, such as in North America, central Europe and across Asia (e.g. Greenland; the Dolomites, Italy; Salt Range, Pakistan; Kashmir, India; Tibet). However, the amount of available data from different disciplines from the same regions and sites is not extensive. For example, the Permian–Triassic transition in the Dolomites (Italy) has an extensive history of palaeontological and sedimentological research (e.g. Broglio Loriga et al., 1988, 1990; Posenato, 2019), but a high-resolution stratigraphic scheme or extensive geochemical investigations are currently lacking. Therefore, to improve our understanding of the Permian–Triassic transition, more interdisciplinary studies are required from different regions and sections.

The Permian–Triassic successions in Türkiye are important for characterising the Permian–Triassic transition, as they largely represent Neotethys oceanic basins, different from the Palaeotethys successions in South China and central Europe. Furthermore, the successions in Türkiye are sedimentologically unique with an extensive anachronistic carbonate response (e.g. Baud et al., 2005; Heindel et al., 2018), and some fossil groups not known from age-equivalent rocks globally (e.g. Dienerian hexactinellid sponge spicules; Kozur et al., 1996). Despite being important in developing our understanding of the Permian–Triassic transition, the successions in Türkiye are still understudied. Many of the key successions in Türkiye are in remote areas and poorly described in previous studies, making them difficult to relocate. In addition to this, the original outcrops of these sections in rural areas have been destroyed over the last few decades. For example, the roads that expose the Taşkent Yolu and Taşkent Şam Deresi sections are being significantly altered, and the previously reported outcrops at Demirtaş are active quarries. Together, this demonstrates the importance of characterising and preserving the Permian–Triassic transition in Türkiye, before key sections are lost by human-induced destruction.

Fieldwork is a fundamental element of geological research, but locating sections and the locations of previous samples is often difficult, which makes reproducing fieldwork challenging. This is partly because of inadequate documentation due to a lack of existing technology in the past and partly because the sections change over time due to weathering or human influence. Assigning different formation names for the same deposits or confusion of lithostratigraphic units can also lead to several disparities between studies (e.g.

20554877, 2026, 2, Downloaded from https://onlinelibrary.wiley.com/doi/10.1002/dep2.70071 by NICE, National Institute for Health and Care Excellence, Wiley Online Library on [14/04/2026]. See the Terms and Conditions (https://onlinelibrary.wiley.com/terms-and-conditions) on Wiley Online Library for rules of use; OA articles are governed by the applicable Creative Commons License

Posenato, 2008) and hinder synthesising data between studies into a consistent stratigraphic framework. There are exceptions, such as the Permian/Triassic boundary GSSP in China (Yin et al., 2001) and the candidate GSSP sections in Hungary (Haas et al., 2007) and Italy (Brandner et al., 2009), where each individual bed has been numbered for decades allowing studies to correlate data collected by different authors (e.g. Farabegoli & Perri, 2012; Foster et al., 2024), but sections like these are exceptions to how fieldwork data is generally shared. Furthermore, fossils and sedimentary structures are often documented in the field and cannot always be sampled. This further poses a risk that unsampled fossils and sedimentary structures are lost over time, and subsequent studies cannot reproduce the data. These issues with fieldwork make it difficult for earth scientists to stick to the FAIR data principles (Findable, Accessible, Interoperable, and Reusable; Wilkinson et al., 2016).

The digitization of outcrops and creation of virtual models, however, allows geoscientists to both document and record fieldwork and sample locations in greater detail, offering great potential in making fieldwork and in situ field data (such as fossil counts and identifications from bedding planes) consistent with the FAIR principles. Geological fieldwork, especially for educational purposes, can be environmentally costly, as travelling can substantially contribute to greenhouse gas emissions and fieldwork involving large groups can result in harming the outcrops. Furthermore, geological fieldwork is not accessible to everyone, due to challenges with the terrain or financial or political reasons (e.g. visa regulations). Virtual outcrop models and digitisation of field data facilitate exploring field sites without visiting the localities directly (e.g. Senger et al., 2022). The invention of affordable unmanned aerial vehicles (UAVs), high-resolution cameras with in-built Lidar, GPS, and 3D modelling software, combined with the development of online platforms not only improves accessibility, but also the reproducibility of field work. Utilising such models for educational purposes can help contributing to meeting net zero target of countries for greenhouse gas emissions (e.g. European Union, 2021).

Here, we document the Permian–Triassic transition in the Antalya and Aladağ Nappes in Türkiye. We demonstrate how UAVs can be used to create virtual models that can be utilised to generate accessible, publicly available virtual field trips and to document fieldwork-related data collection. The Antalya and Aladağ Nappes in Türkiye are ideal regions to create virtual field guides as these Nappes hold records of major ecological and environmental changes associated with the Permian–Triassic transition (Baud et al., 2009). Our new synthesis includes and incorporates additional sections and allows for making pre-existing data consistent with FAIR principles, as previously provided GPS coordinates and section names were checked for their accuracy and replaced by a single GPS coordinate and unique name for each section, removing duplicate naming and inaccurate location information.

2 | GEOLOGICAL SETTING

We have digitised and sampled 10 different sections at four locations (Çürük Dağ Crest, Çürük Dağ Cliff, Çürük Dağ Valley, Öznurtepe Creek, Öznurtepe Road, Demirtaş, Taşkent Yolu, Taşkent Yolu Hill, Taşkent Şam Deresi and Taşkent Şam Deresi Hill; Figure 1, Table 1). The sedimentary successions in these places belong to two allochthonous tectono-stratigraphic units of the Tauride Block, namely the Antalya Nappe (Çürük Dağ, Öznurtepe, Demirtaş in Antalya) and the Aladağ Nappe (Taşkent in Konya) (Altıner et al., 2000, 2021; Özgül, 1984, 1997).

Starting around the Permian–Triassic transition, the tectonic units of Türkiye became tectonically active and were transformed as it marked the junction between the opening of the Neotethys Ocean and the subduction of the Palaeotethys Ocean (Şengör & Yılmaz, 1981). During the Permian, the tectonic units of Türkiye are interpreted as having been deposited along the northern margin of Gondwana, facing the Palaeotethys Ocean. The Palaeotethys Ocean was actively subducted to the north, and the studied sedimentary successions were considered to be part of a large carbonate platform (Altıner et al., 2000; Robertson et al., 2012). The Upper Permian platform carbonates of the studied localities are attributed to the Southern Biofacies Belt, which is confined by the foraminifera genera *Paradagmarita* and *Shanita* and extends from Türkiye to Iran, Saudi Arabia, Oman, western Yunnan, Myanmar and western Thailand (Altıner et al., 2000).

During the Permian–Triassic transition, the successions from the Antalya Nappe (Çürük Dağ in Kemer; Öznurtepe in Gazipaşa; and Demirtaş) are considered to be deposited on a southward facing carbonate platform in the newly rifting basin of the Neotethys Ocean, whilst successions from the Aladağ Nappe (Taşkent in Konya) are considered to be deposited on the northern side of the carbonate platform towards the Palaeotethys Ocean (Altıner et al., 2000: fig 8; Stampfli et al., 1991). During the Triassic, this carbonate platform is interpreted to have ruptured to produce extensional basins, with the Antalya Nappe becoming isolated on the northern margin of the Neotethys, whilst the Aladağ Nappe was part of the Tauride-Anatolide carbonate platform facing the southern side of the Inner Tauride Ocean by the Late Triassic (Robertson et al., 2004, 2012). Main rifting of the Antalya Nappe occurred during the Anisian–Ladinian transition (Şengör & Yılmaz, 1981)

20554877, 2026, 2, Downloaded from https://onlinelibrary.wiley.com/doi/10.1002/dep2.70071 by NICE, National Institute for Health and Care Excellence, Wiley Online Library on [14/04/2026]. See the Terms and Conditions (https://onlinelibrary.wiley.com/terms-and-conditions) on Wiley Online Library for rules of use; OA articles are governed by the applicable Creative Commons License

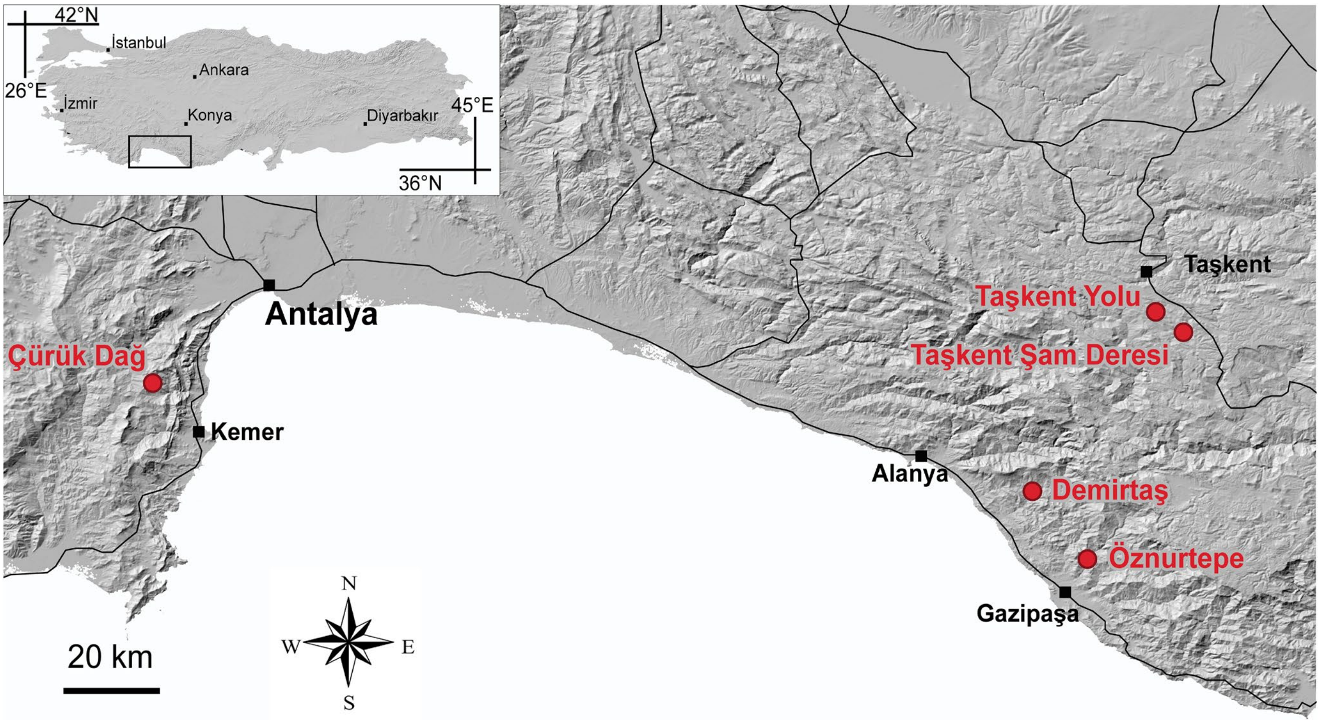

FIGURE 1 The locations of studied sections in southwest Türkiye.

with an onset during the Permian (Şahin & Altıner, 2019). Hence, the sedimentary successions during the Permian–Triassic transition were affected by the tectonic evolution of the Tethyan ocean basins.

2.1 | Çürük Dağ

The Middle–Upper Permian at Çürük Dağ is represented by the Pamucak Formation (Lys & Marcoux, 1978) which consists of a ca. 1000 m thick carbonate succession (Baud et al., 2009, fig. 14). The Changhsingian deposits of the Pamucak Formation were previously considered to be 12 m thick (Richoz, 2006), as indicated by the foraminifera *Paradagmarita monodi* Lys in Lys & Marcoux, 1978, and a low diversity brachiopod assemblage dominated by *Spinomarginifera* and *Orthothetina*, and *Hindeodus* cf. *praeparvus* (Kozur, 1996) (Angiolini et al., 2007). However, the Changhsingian is now considered to be more than 100 m thick, based on the presence of the index fossil *Paradagmarita monodi* Lys in Lys & Marcoux, 1978 (Baud in Baud et al., 2009: 8). The nodular limestone of the uppermost part of the Permian Pamucak Formation is overlain by a 30 cm thick oolite bed and stromatolites of the Lower Triassic Kokarkuyu Formation (Altıner & Zaninetti, 1981; Baud et al., 2005, 2009; Marcoux & Baud, 1988). The earliest Triassic has been assigned to the lowermost microbialites based on the presence of the conodonts *Hindeodus parvus* (Kozur & Pjatakova, 1976) and *Isarcicella isarcica staeschei* (Dai & Zhang, 1989) (Crasquin-Soleau et al., 2002; Richoz, 2006). Thirty-one metres above the base of the Kokarkuyu Formation, within the oolitic beds, the conodont *Isarcicella lobata* indicating the second zone of the Griesbachian has been found (Angiolini et al., 2007).

Şenel (1997) assigned the Upper Permian deposits around Çürük Dağ to the Dinek Formation (Dinek Limestones: Kalafatçıoğlu, 1973), which has a type section in Sivridağ located north-west of Çürük Dağ. According to Kalafatçıoğlu (1973), the Dinek Limestones attain 200 m thickness in their type locality but reach over 1000 m in thickness in total. The Dinek Limestones are overlain by the Permian Fesliğen Dolomites, which underlie the Triassic sandstones (Kalafatçıoğlu, 1973). The information on the faunal content of the Dinek Formation and the stratigraphic succession in its type locality is limited and needs to be updated to assess its relationship to the Pamucak Formation defined by Lys and Marcoux (1978). The present information is not adequate to clarify whether they represent two distinct formations or whether they are synonyms used for the laterally continued deposits. If they represent the same deposit, the Dinek Formation has priority for usage, as it was defined prior to the Pamucak Formation. Şenel (1997) used the name Kesmeköprü Formation for the Lower Triassic deposits at Çürük Dağ, but this name cannot be traced in the literature, even in the references that were provided by Şenel (1997), therefore is considered a *nomen nudum*.

20554877, 2026, 2, Downloaded from https://onlinelibrary.wiley.com/doi/10.1002/dep2.70071 by NICE, National Institute for Health and Care Excellence, Wiley Online Library on [14/04/2026]. See the Terms and Conditions (https://onlinelibrary.wiley.com/terms-and-conditions) on Wiley Online Library for rules of use; OA articles are governed by the applicable Creative Commons License

2.2 | Demirtaş and Öznurtepe

The Upper Permian deposits at Demirtaş and Öznurtepe belong to Yüğlük Tepe Limestone (Özgül, 1985), which yields the uppermost Changhsingian inferred by *Paradagmarita monodi* Lys in Lys & Marcoux, 1978 (Groves et al., 2005; Özgül, 1985). The Yüğlük Tepe Limestone is overlain by the Sapadere Formation (Özgül, 1985). The lower members of the Sapadere Formation, the Beslengiler Limestone Member and Taşlıca Member, were assigned to the Scythian (= Early Triassic) based on the presence of the foraminifera *Postcladella kalhori* (Brönnimann et al., 1972), and the molluscs *Unionites fassaensis* (Wismann in Münster, 1841), *Claraia* sp. and *Ladinaticella costata* (Münster, 1841) (Groves et al., 2005; Özgül, 1985). The Beslengiler Limestone Member starts with a thin oolite bed and continues with overlying stromatolites and oolite successions (Baud et al., 2009; Özgül, 1985; Richoz, 2006). The Taşlıca Member comprises varicoloured mudstone and marl alternations (Özgül, 1985).

Lower Triassic successions at Demirtaş and Öznurtepe were previously also assigned to the Kokarkuyu Formation (Altıner, 1981; Altıner et al., 2021) and partly to the Akıncıbeli Formation at Demirtaş (Şahin & Altıner, 2019). The Akıncıbeli Formation was used in an unpublished report by Demirtaşlı in 1987 (Şahin & Altıner, 2019) and later than the description of the Sapadere Formation (Özgül, 1985); hence, it needs to be abandoned. The Beslengiler Limestone Member and Taşlıca Member might be junior synonyms of the Kokarkuyu Formation; however, the original description of the Kokarkuyu Formation only encompasses the Griesbachian microbialites and oolites, and the yellow Dienerian mudstones (Altıner & Zaninetti, 1981), but not the Olenekian grey to red siliciclastics and yellow mudstones with *Ladinaticella costata* (Özgül, 1985).

The Lower Triassic rocks in Antalya Nappes were assigned in some publications to the Katarası Formation (e.g. Şenel et al., 2016), which was later regarded as a group by Altıner et al. (2024). The Katarası Formation was named in an unpublished report by Demirtaşlı (1967); hence, it is not a formally established name and should be abandoned (Özgül et al., 1973).

2.3 | Taşkent

At Taşkent, the Upper Permian is represented by the Çekiç Dağı Formation, which yields algal and foraminiferal limestone deposits overlain by an oolite bed (Özgül, 1997). The Yellice Member of the Çekiç Dağı Formation represents the Upper Permian in Taşkent (Özgül, 1997). The Changhsingian age is assigned based on the foraminifera *Paradagmarita monodi* Lys in Lys & Marcoux, 1978 (Groves et al., 2005; Payne et al., 2007). The Changhsingian sequence in Taşkent reaches up to ca. 50 m in thickness (Altıner et al., 2021). The Çekiç Dağı Formation is overlain by the Triassic Gevne Formation (Özgül, 1997). The lowermost İspatlı Member of the Gevne Formation consists of stromatolites and oolites in the lower part, and mudstone–limestone alternations above them. This member is considered Lower Triassic due to the presence of taxa such as the foraminifera *Postcladella kalhori* (Brönnimann et al., 1972), and molluscs *Unionites fassaensis* (Wismann in Münster, 1841), *Claraia clarae* (Emmrich, 1844) and *Ladinaticella costata* (Münster, 1841) (Groves & Altıner, 2005; Özgül, 1997; Ünal et al., 2003). The thickness of the Lower Triassic rock succession reaches 600 m in Taşkent (Groves et al., 2005), and up to 715 m in its type section (Özgül, 1997).

2.4 | Position of the Permian/Triassic boundary and formation boundaries

The Permian/Triassic boundary was constrained only in the Çürük Dağ section. The transitional oolites record the uppermost Changhsingian conodont *Hindeodus* cf. *praeparvus* (Kozur, 1996) (Angiolini et al., 2007) and the subsequent lowermost microbialite bed records the index fossil conodont *Hindeodus parvus* (Kozur & Pjatakova, 1976) (Crasquin-Soleau et al., 2002; Richoz, 2006). The Permian/Triassic boundary in all other sections is placed based on lithological correlations, overall fossil content (e.g. Changhsingian marker *Paradagmarita monodi*; Early Triassic marker *Postcladella kalhori*) and the negative carbon isotope excursion reported in the transitional oolites in all sections (e.g. Richoz, 2006). Accordingly, the Permian/Triassic boundary is placed at the contact between Changhsingian oolite and Griesbachian stromatolite beds (Angiolini et al., 2007; Groves et al., 2005; Payne et al., 2007; Varol et al., 2011). Furthermore, $\delta^{13}C$ declines from 4‰ to 0‰–2‰ near the formation boundaries in the transitional oolites in all sections (Frank et al., 2025; Lau et al., 2016; Richoz, 2006), consistent with the global carbon cycle perturbation observed across the Permian–Triassic transition (Baud et al., 1989; Korte & Kozur, 2010). There is a need for further studies involving conodont biostratigraphy and geochronology to corroborate the position of the Permian/Triassic boundary. Studies are also needed for locating the Wuchiapingian/Changhsingian boundary and Early Triassic stage boundaries.

One of the confusions in the published literature is the position of formation boundaries. Nearly all studies place formation boundaries above the transitional

20554877, 2026, 2, Downloaded from https://onlinelibrary.wiley.com/doi/10.1002/dep2.70071 by NICE, National Institute for Health and Care Excellence, Wiley Online Library on [14/04/2026]. See the Terms and Conditions (https://onlinelibrary.wiley.com/terms-and-conditions) on Wiley Online Library for rules of use; OA articles are governed by the applicable Creative Commons License

oolites in the studied formations (Groves et al., 2005; Baud et al., 2005, 2009; Richoz, 2006; Payne et al., 2007; Altıner et al., 2021, 2024). However, Özgül (1985) placed the formation boundary below the transitional oolites and described a thin oolitic bed in the Sapadere Formation in its type section near Demirtaş. In Taşkent, Özgül (1997) included the oolite bed in the Yellice Limestone Member of the Çekiç Dağı Formation; hence, in Taşkent, the transitional oolites, by definition, are below the formation boundary. The transitional oolites were neither described in the Upper Permian Pamucak Formation by Lys and Marcoux (1978) nor in the Lower Triassic Kokarkuyu Formation by Altıner and Zaninetti (1981). Subsequently, it was included in the Kokarkuyu Formation by Marcoux and Baud (1988), but then in the Pamucak Formation (Baud et al., 2005, 2009; Richoz, 2006; Altıner et al., 2021, 2024).

The oolitic beds mark an abrupt change in the environment and the onset of a significant decline in biodiversity, so the facies change from skeletal carbonates (packstones/wackestone) to poorly fossiliferous oolites and microbialites. This transition is remarkably consistent with observations from the base of the Werfen Formation in Italy (Farabegoli et al., 2007; Ünal et al., 2003). Furthermore, the preservation and size of the ooids within the oolitic transitional bed are consistent with the oolitic beds of the Kokarkuyu and Gevne formations. For these reasons, we herein included the first oolite bed in the younger formations under the informal name 'transitional oolites' as it represents the transition from the Permian to the Triassic and marks the onset and deposition during the extinction event.

3 | METHODS

In the studied locations, we measured sections across the Permian/Triassic boundary for stratigraphic logging and took rock samples for palaeontological, sedimentological, organic geochemical and inorganic geochemical analyses. The detailed results of the geochemical analyses are published in separate articles (Buchwald et al., 2025; Frank et al., 2025) and the palaeontological analyses are currently being prepared for publication. All rock and fossil samples figured herein are housed at the Natural History Museum, Ankara under the collection name BK-2024.

A commercial unmanned aerial vehicle (UAV, DJI Mini4pro with an 1/1.3-inch CMOS, effective pixels: 48 MP, weight <250 g) was used for the photograph acquisition. Using a manual terrain-following flight method, aerial photographs were taken with forward and lateral overlap rates both >70%. During the data preprocessing and verification phase, images exhibiting focus blur, abnormal exposure or invalid regions were filtered out to ensure data quality. To enhance modelling accuracy and efficiency, a multi-phased, cross-software processing method was adopted:

Agisoft Metashape Pro was first employed with the alignment accuracy set to high, reference preselection set to 'source' or 'estimated', and a key point limit of 40 000 to perform aerial triangulation:

- Taşkent Yolu model, 1784 out of 2750 photographs were aligned, generating 743 648 tie points.
- Demirtaş model, 1468 out of 1487 photographs were aligned, generating 849 843 tie points.
- Öznurtepe Creek model, 2194 out of 2804 photographs were aligned, generating 1 184 433 tie points.
- Öznurtepe Road model, 365 out of 1228 photographs were aligned, generating 142 265 tie points.
- Çürük Dağ Crest, Cliff and Valley model (6072 photographs) achieved full alignment using the estimation algorithm, generating 1,905,737 tie points.
- Taşkent Şam Deresi model (8651 photographs) achieved full alignment using the estimation algorithm, generating 4,465,031 tie points.

After the aerial triangulation of each dataset, an XML file containing camera parameters and image control points data were exported for subsequent modelling in iTwin Capture. Aerial triangulation reports were also generated for detailed inspections. This dual-software workflow effectively improved model warping and stratification problems.

In the multi-view bundle adjustment phase, image indexing was achieved through a hierarchical pyramid matching algorithm based on GNSS/IMU orientation systems combined with multi-view geometry principles. Perspective distortions inherent in oblique imagery were corrected using control-point-constrained error equations. Dense matching utilises multi-primitive algorithms and high-occlusion detection techniques to improve homologous point matching in complex terrains or objects. Subsequently, irregular triangular meshes were built using octree subdivision or region-growing methods, with dynamic adjustment of triangle density to generate high-precision digital surface models. Finally, texture mapping was performed through coordinate transformation and colour matching to accurately project 2D image colour onto the 3D mesh, yielding both realistic untextured (white) and textured models.

The final model outputs are: Demirtaş model (5.71 GB, 14 tiles), Öznurtepe Creek model (4.05 GB, 18 tiles), Öznurtepe Road model (863 MB, 1 tile), Çürük Dağ Crest, Cliff and Valley model (12.9 GB, 44 tiles), Taşkent Yolu model (4.46 GB, 16 tiles) and Taşkent Şam Deresi model (31.8 GB, 89 tiles). The outcrop models have been uploaded to Zenodo for download and can be visualised in software

20554877, 2026, 2, Downloaded from https://onlinelibrary.wiley.com/doi/10.1002/dep2.70071 by NICE, National Institute for Health and Care Excellence, Wiley Online Library on [14/04/2026]. See the Terms and Conditions (https://onlinelibrary.wiley.com/terms-and-conditions) on Wiley Online Library for rules of use; OA articles are governed by the applicable Creative Commons License

20554877, 2026, 2, Downloaded from https://onlinelibrary.wiley.com/doi/10.1002/dep2.70071 by NICE, National Institute for Health and Care Excellence, Wiley Online Library on [14/04/2026]. See the Terms and Conditions (https://onlinelibrary.wiley.com/terms-and-conditions) on Wiley Online Library for rules of use; OA articles are governed by the applicable Creative Commons License

TABLE 1 The GPS points of the logged and modelled sections.

Section	Latitude	Longitude	Altitude (m)	Digital model
Çürük Dağ Crest	N36°41.543	E030°27.681	1429	https://outcrop3d.deep-time.org/?model=a52519f2-ff78-ea42-6403-42f5022c8e31
Çürük Dağ Cliff	N36°41.537	E030°27.556	1409	
Çürük Dağ Valley	N36°41.568	E030°27.460	1306	
Öznurtepe Road	N36°19.972	E032°21.602	126	https://outcrop3d.deep-time.org/?model=fd1234a8-a099-6f92-61a9-ab64c907ed4d
Öznurtepe Creek	N36°19.890	E032°21.474	65	https://outcrop3d.deep-time.org/?model=9cc59e1d-fcb6-b6ce-1912-bd017d00749e
Demirtaş	N36°28.821	E032°15.038	409	https://outcrop3d.deep-time.org/?model=ec2a8188-27b3-1da2-47b1-302f67660205
Taşkent Şam Deresi	N36°47.994	E032°33.461	1642	https://outcrop3d.deep-time.org/?model=05b1d3a7-7d7e-684b-8005-8b774090b52e
Taşkent Şam Deresi Hill	N36°48.335	E032°33.258	1841	Unavailable
Taşkent Yolu	N36°50.615	E032°30.023	1902	https://outcrop3d.deep-time.org/?model=16ad6c91-681e-d0a8-2afd-55d57ebf489f
Taşkent Yolu Hill	N36°50.967	E032°30.067		Unavailable

such as DasViewer (https://doi.org/10.5281/zenodo.16366010; https://doi.org/10.5281/zenodo.16363427). All models have been visualised on Outcrop3D, a non-commercial web-based digital outcrop platform (Wang et al., 2024; Table 1). Finally, we have annotated the openly available models on Outcrop3D with pictures from field observations, which are also present in the Appendices.

4 | PERMIAN–TRIASSIC TRANSITION IN TÜRKIYE

4.1 | Çürük Dağ

The Çürük Dağ section corresponds to a mountain situated at the head of the Göynük Valley, near Üçoluk village and ca. 15 km NW of Kemer (Figures 1 and 3). The Permian–Triassic transition is exposed on the southern flank of Çürük Dağ. The model includes the three outcrops described in this study: Çürük Dağ Crest, Çürük Dağ Cliff and Çürük Dağ Valley (Figure 2, Table 1). Of the three exposures, Çürük Dağ Crest is the easiest to access and safest, whilst severe injuries in previous expeditions are known from Çürük Dağ Valley, and Çürük Dağ Cliff is located on a steep slope where a slip or a fall would be life threatening.

The upper part of nearly 1000 m thick Middle–Late Permian Pamucak Formation (Baud et al., 2009) comprises dark-grey, fossil-rich carbonates which are classified as mostly wackestones and packstones yielding two levels of carbonate rosettes (or carbonate crystal fans, see Appendix 6) and abundant fossils, including brachiopods, calcareous algae, bryozoans, foraminifera, gastropods, ostracods and echinoderms (Brachiopoda: Angiolini et al., 2007; Verna et al., 2011; Trilobita: Lerosey-Aubril & Angiolini, 2009; Ostracoda: Crasquin-Soleau et al., 2002, 2004). Higher up along the succession, the limestone becomes nodular (Figure 4; Appendix 1-Figure 37). The limestones bear bellerophontids, the brachiopods *Spinomarginifera* and *Orthothetina*, bryozoans and large calcareous algae (Figure 5H,I,J,K,L,M). The scree deposits, originating from

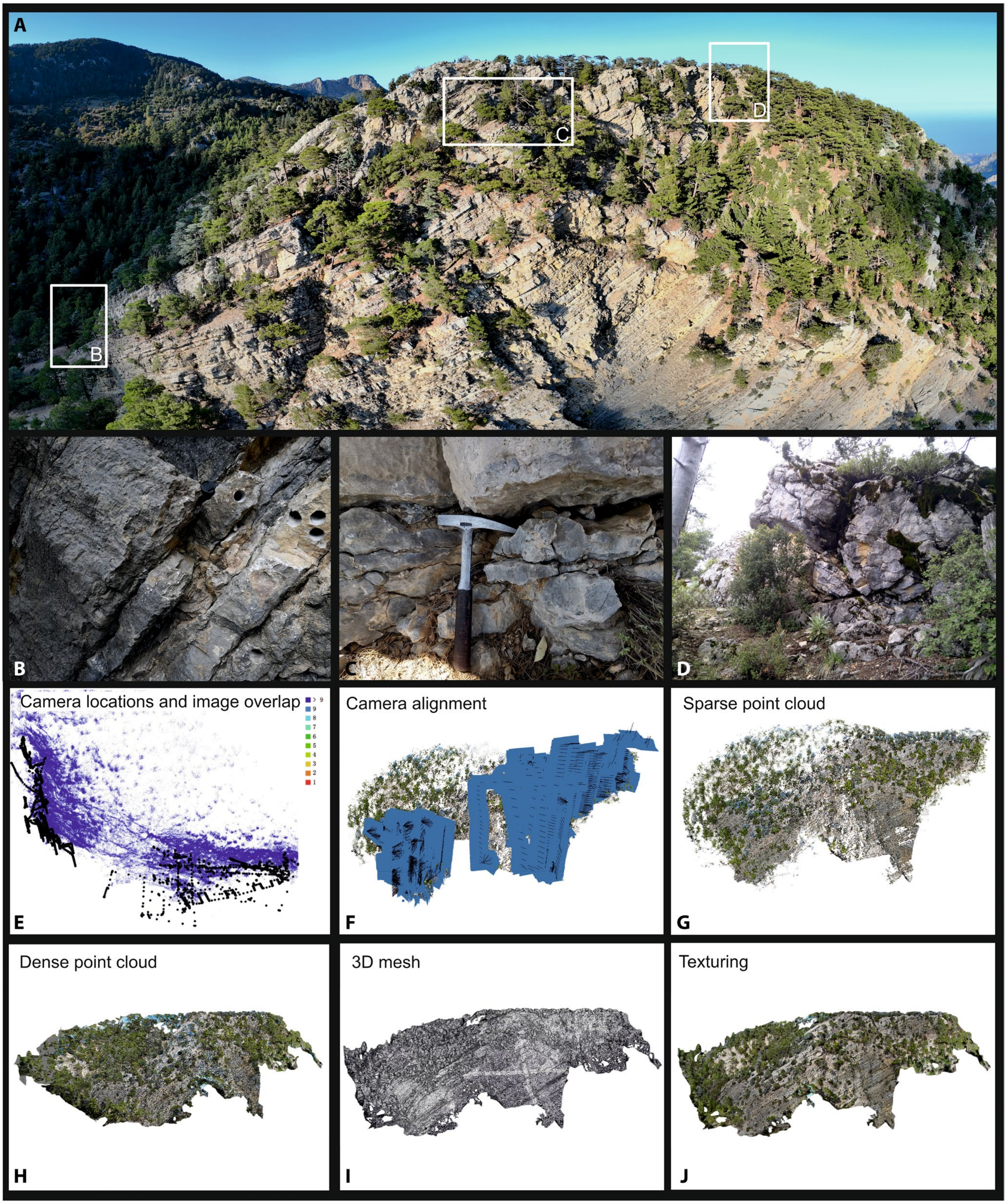

FIGURE 2 (A) Panoramic aerial photograph of Çürük Dağ, the white boxes indicating the studied sections. (B) Çürük Dağ Valley section. (C) Çürük Dağ Cliff section, the head of the hammer is at the last nodular limestone bed just below the transitional oolites. (D) Çürük Dağ Crest section. (E–J) Image processing workflow to create the virtual outcrop model of the Çürük Dağ sections.

the Pamucak Formation in the Valley section, are dominated mainly by the two brachiopod genera, bellerophontids, and burrow fragments up to 2 cm in diameter. The scree material contains few infaunal bivalves including *Edmondia* and the pseudorthoceratid *Lopingoceras lopingense*. In the scree, it is also possible to find carbonate rosettes.

20554877, 2026, 2, Downloaded from https://onlinelibrary.wiley.com/doi/10.1002/dep2.70071 by NICE, National Institute for Health and Care Excellence, Wiley Online Library on [14/04/2026]. See the Terms and Conditions (https://onlinelibrary.wiley.com/terms-and-conditions) on Wiley Online Library for rules of use; OA articles are governed by the applicable Creative Commons License

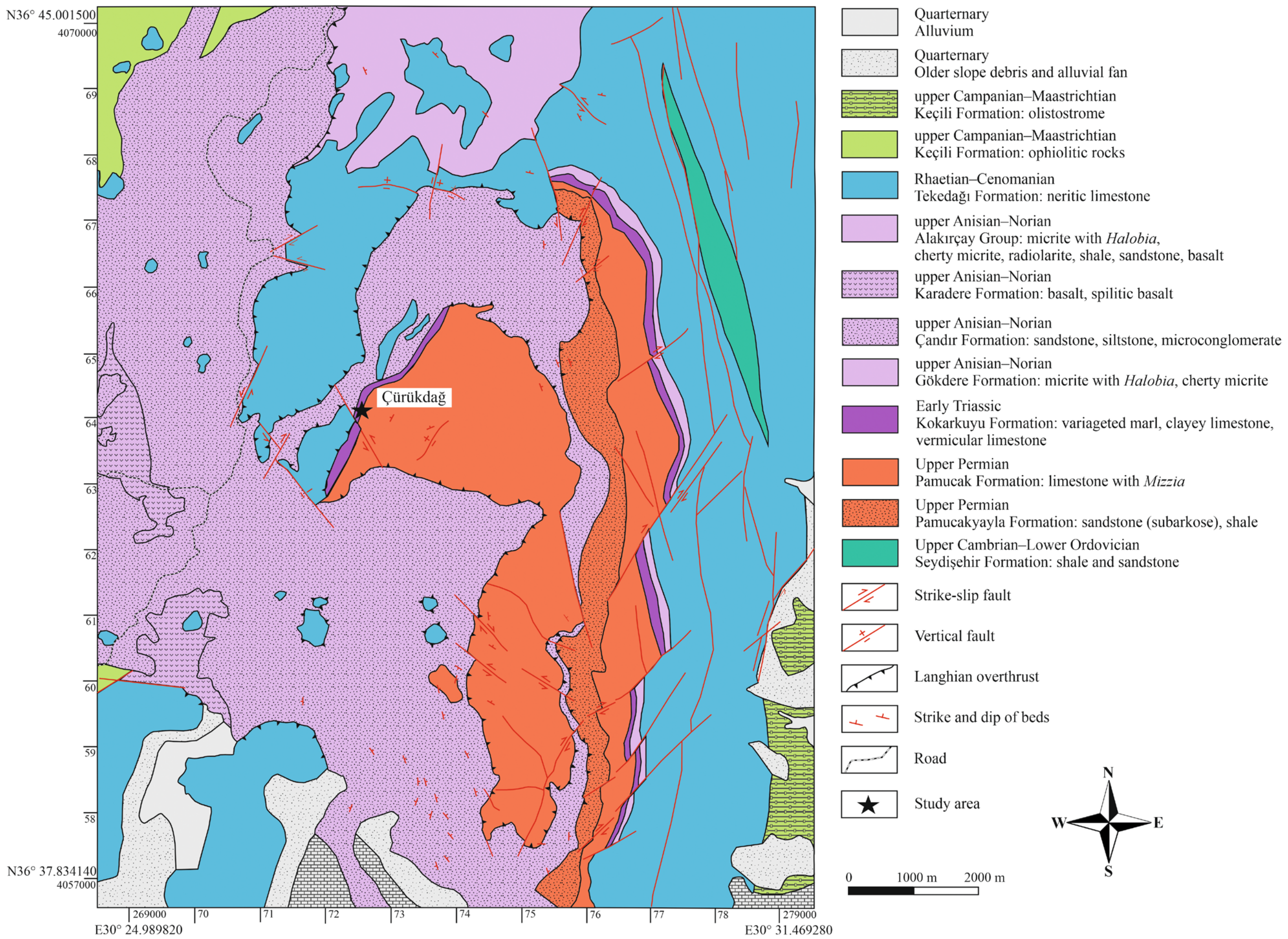

FIGURE 3 Geological map of the region around the study area in Çürük Dağ (modified after MTA 1:25.000 scale maps). Coordinates are given in Universal Transverse Mercator (Zone 36S) and in World Geodetic System (WGS1984).

Above the nodular limestones, the lithofacies abruptly changes into oolitic grainstones (Figure 5G; Appendix 1-Figure 40). The formation boundary is poorly defined and inconsistent between different studies (e.g. compare Baud et al., 2009; Marcoux & Baud, 1988). We have marked the base of the transitional oolites as the formation boundary following Marcoux and Baud (1988) as it represents an abrupt facies change. The transitional oolites were deposited on an erosional surface (Kershaw et al., 2011) and within the transitional oolite bed, flat pebbles were observed (Appendix 1-Figure 38). The oolite bed is overlain by microbialites and stromatolites (Baud et al., 2005; Kershaw et al., 2011, 2012), but in the Çürük Dağ Crest section, there is a thin carbonate mudstone layer (10 cm thick) between the oolite bed and the stromatolites (Figure 4), which is probably the discontinuous bed identified as thrombolites by Kershaw et al. (2012). A Griesbachian age has been assigned to the microbialites based on the presence of the conodonts *Hindeodus parvus* and *Isarcicella isarcica staeschei* (Crasquin-Soleau et al., 2002; Richoz, 2006). The first 16 m of the microbialites of the Kokarkuyu Formation are characterised by thrombolites and domal stromatolites (Kershaw et al., 2012; Appendix 1-Figure 34). Lipid biomarker data suggests that the layered microbial mats forming these microbialites were probably cyanobacteria-dominated, with anoxygenic photoautrophic bacteria and sulfate-reducing bacteria inhabiting anoxic zones within the microbial mat (Heindel et al., 2018). Microbialites are overlain by dolomitized, oolitic grainstones which have sparse fossil content but yield ostracods (Forel, 2015) and bivalves (Figure 5F).

The microbialite–oolitic (microbial) unit of the Kokarkuyu Formation transitions abruptly into light-yellow coloured mixed siliciclastic-carbonate mudstones that yield a low diversity of cosmopolitan mollusc genera *Neoschizodus*, *Claraia*, *Eumorphotis* (Figure 5C,D) and a new myophoricardiid bivalve genus that resembles *Unionites* in external shell morphology

20554877, 2026, 2, Downloaded from https://onlinelibrary.wiley.com/doi/10.1002/dep2.70071 by NICE, National Institute for Health and Care Excellence, Wiley Online Library on [14/04/2026]. See the Terms and Conditions (https://onlinelibrary.wiley.com/terms-and-conditions) on Wiley Online Library for rules of use; OA articles are governed by the applicable Creative Commons License

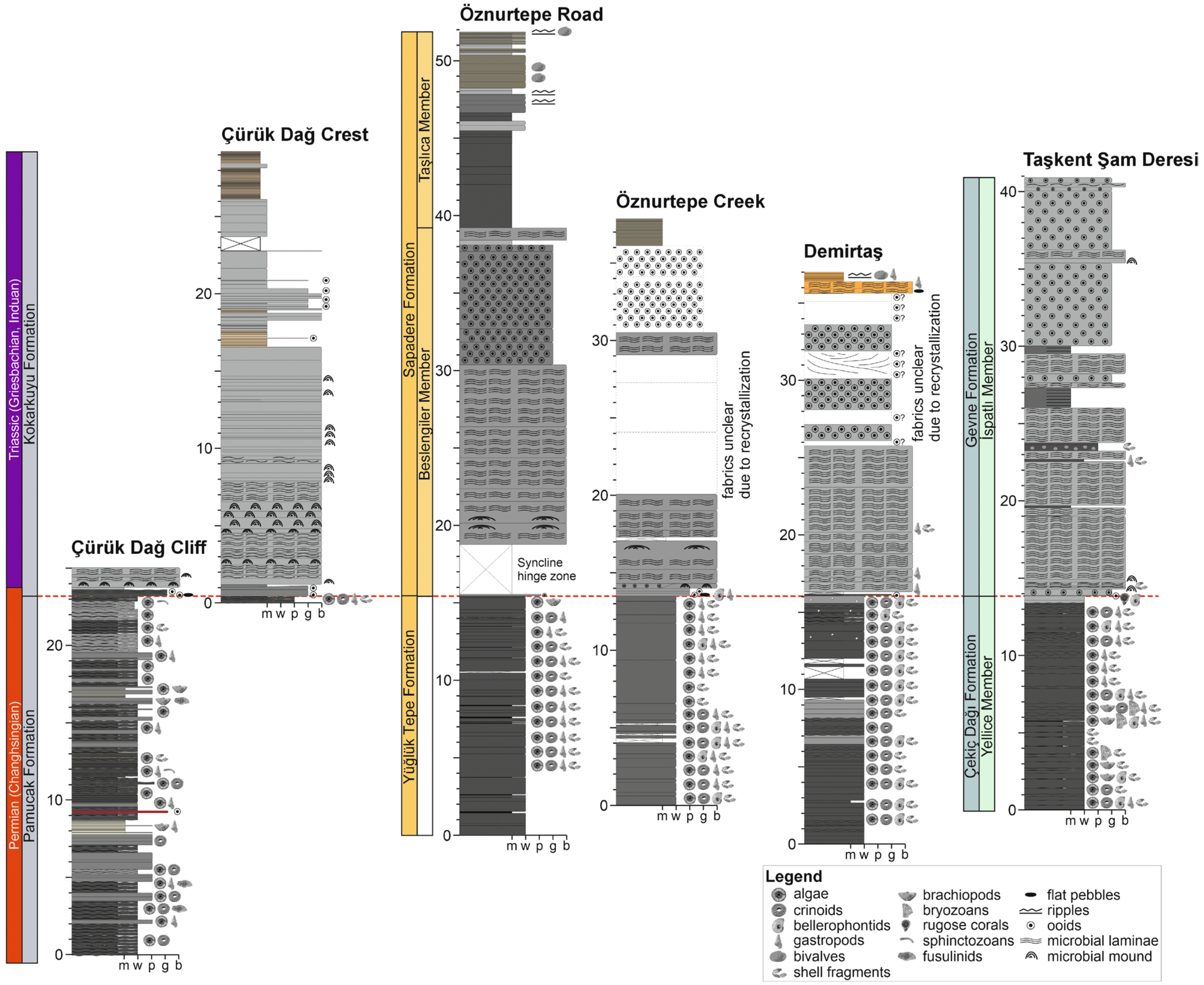

FIGURE 4 Detailed log of the studied sections showing palaeontological and lithological observations made in the field. The colour represents the rock colours and the red dashed line indicates the formation boundary; m = mudstone, w = wackestone, p = packstone, g = grainstone and b = bindstone.

(Appendix 1-Figures 16 and 17). The Lower Triassic yellow mudstones of the Kokarkuyu Formation are best exposed in the Çürük Dağ Valley section, whilst they are only exposed as small pieces of scree on the crest. This unit is overlain by varicoloured siliciclastic–carbonate mudstones that are characterised by thin bedding (typically 1–5 cm), microgastropod and bivalve dominated shell beds (tempestites), occasional pyrite deposits, shelf-filled gutter casts, flat pebble conglomerates, cross-bedding and asymmetrical ripple marks (Figures 5A,B,E; Appendix 1-Figures 19–29). The fossil content and sedimentary structures of this unit resemble lithofacies deposited on a homoclinal ramp and are very similar to the lithofacies recorded from the Werfen Formation in central Europe (e.g. Broglio Loriga et al., 1990; Hips, 1998).

4.2 | Demirtaş

The Demirtaş exposures are 10 km north-east of Demirtaş on the Sapadere Creek (Figures 1 and 6). The Permian–Triassic transition in this area was first described in detail by Özgül (1985) who named the Yüğlük Tepe and Sapadere Formation for the Upper Permian and Lower Triassic, respectively. Here, the measured sections are located in the type region of these formations and near the section named as Demirtaş-Kuşdavut by Richoz (2006), and ca. 1 km south-west of the Tırlar section measured by Şahin and Altıner (2019). The studied Permian–Triassic transition is located slightly north of a small limestone quarry, which is next to the road that diverged from Kaşlıoğlu Street and leads to the Yaylakonak Neighbourhood. The Permian/

20554877, 2026, 2, Downloaded from https://onlinelibrary.wiley.com/doi/10.1002/dep2.70071 by NICE, National Institute for Health and Care Excellence, Wiley Online Library on [14/04/2026]. See the Terms and Conditions (https://onlinelibrary.wiley.com/terms-and-conditions) on Wiley Online Library for rules of use; OA articles are governed by the applicable Creative Commons License

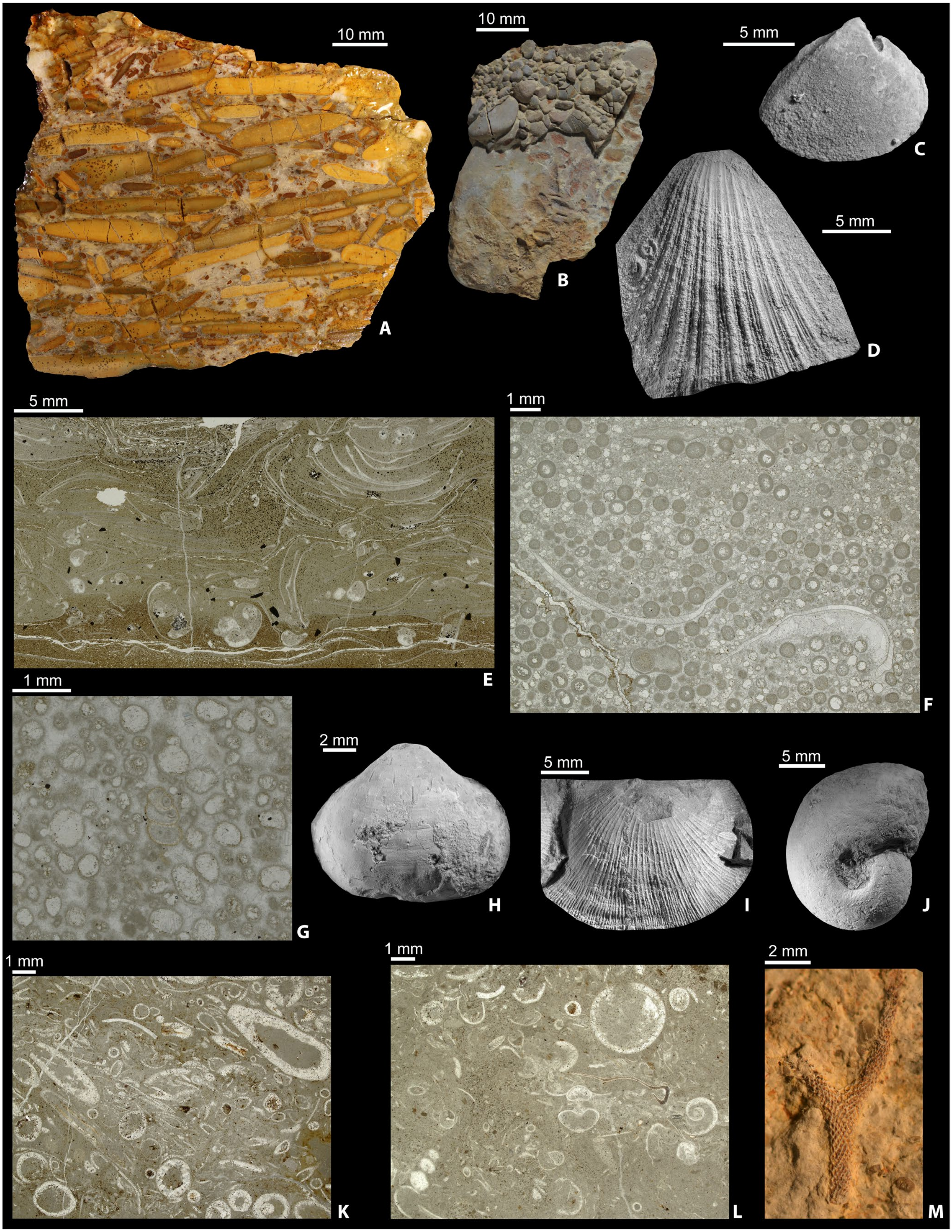

20554877, 2026, 2, Downloaded from https://onlinelibrary.wiley.com/doi/10.1002/dep2.70071 by NICE, National Institute for Health and Care Excellence, Wiley Online Library on [14/04/2026]. See the Terms and Conditions (https://onlinelibrary.wiley.com/terms-and-conditions) on Wiley Online Library for rules of use; OA articles are governed by the applicable Creative Commons License

FIGURE 5 Sedimentary structures, fossils and facies at Çürük Dağ. (A) Polished section of flat pebbles containing yellow mudstone rip-up clasts, Dienerian, Kokarkuyu Formation, BK-2024/667a. (B) Flat pebbles containing yellow mudstone rip-up clasts, Dienerian, Kokarkuyu Formation, BK-2024/667b. (C) *Neoschizodus ovatus* (Goldfuss, 1837), Dienerian, Kokarkuyu Formation, BK-2024/534. (D) *Eumorphotis inaequicostata* (Benecke, 1876) in yellow mudstone beds, with two encrusting microconchids, Dienerian, Kokarkuyu Formation, BK-2024/47. (E) Tempestite in yellow mudstone beds, includes thin shelled bivalves, gastropods and pyrite crystals (appear in dark), Dienerian, Kokarkuyu Formation, TSCV_1. (F) Oolite bed with *Neoschizodus* shells, which underlies the yellow mudstone layer, Griesbachian, Kokarkuyu Formation, TSCCr_1. (G) Oolite bed with *Coelostylina* sp., which underlies the yellow mudstone layer, Griesbachian, Kokarkuyu Formation, TSCCr_1. (H) *Spinomarginifera* sp. Changhsingian, Pamucak Formation, BK-2024/31. (I) *Orhothetina ladina* (Stache, 1878), Changhsingian, Pamucak Formation, BK-2024/58a. (J) Bellerophontida indet. sp., Changhsingian, Pamucak Formation, BK-2024/64. (K) Packstone with *Gymnocodium* sp. just below the transitional oolites, Changhsingian, Pamucak Formation, TSCV_7. (L) Wackestone with bellerophontid gastropods, trilobite, *Gymnocodium* sp., foraminifera, Changhsingian, Pamucak Formation, TSCCl_2. (M) Bryozoa, Changhsingian, Pamucak Formation, BK-2024/662.

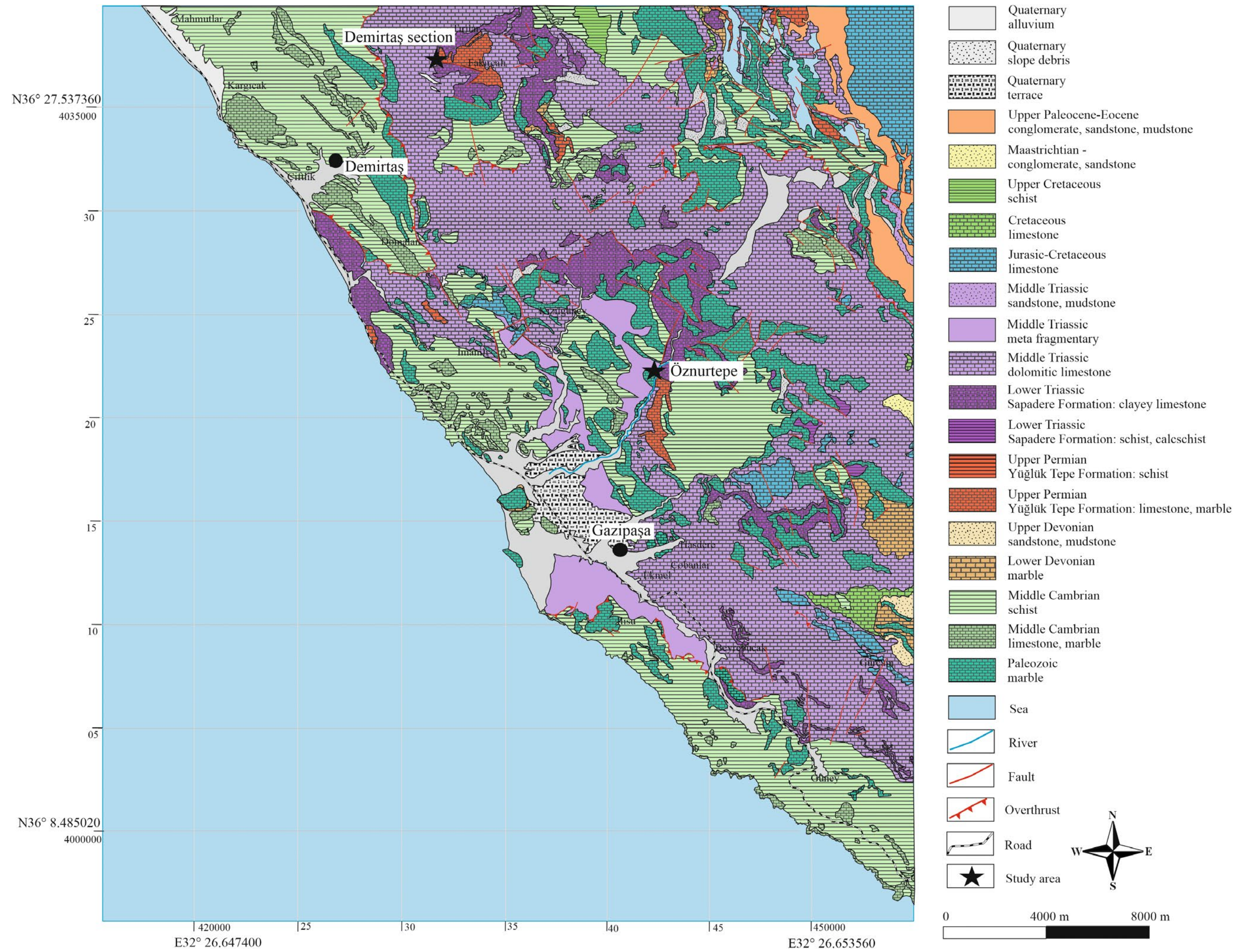

FIGURE 6 Geological map of the region around the study area in Demirtaş and Öznurtepe (modified after MTA 1:100.000 scale maps). Coordinates are given in Universal Transverse Mercator (Zone 36S) and in World Geodetic System (WGS1984).

Triassic boundary is well-exposed at the studied section, which is in a wooded area (Figure 7A, Table 1). In addition, there are two other sites exposing the Permian–Triassic transition located in this area. At the lower part of a small quarry (N36°28.7787, E032°14.9169, Alt. 200 m), as well as in the upper part of the large quarry (Baud et al., 2009; Appendix 5), but because of the freshly cut surfaces in the two quarries, it is difficult to discern sedimentological features. In addition, the two quarries are active, and therefore inaccessible. On the southern side of the road, between the small northern quarry and the larger southern quarry there

20554877, 2026, 2, Downloaded from https://onlinelibrary.wiley.com/doi/10.1002/dep2.70071 by NICE, National Institute for Health and Care Excellence, Wiley Online Library on [14/04/2026]. See the Terms and Conditions (https://onlinelibrary.wiley.com/terms-and-conditions) on Wiley Online Library for rules of use; OA articles are governed by the applicable Creative Commons License

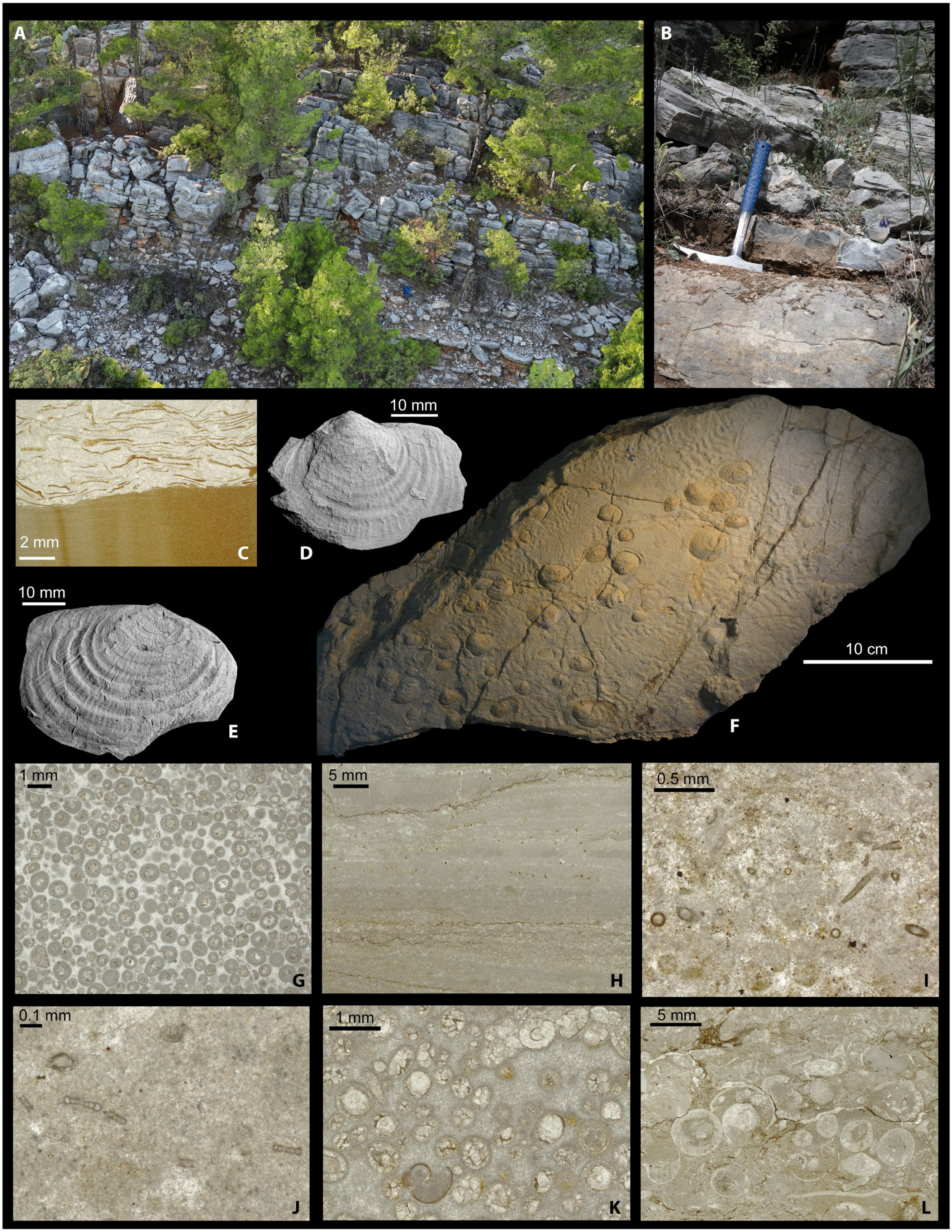

20554877, 2026, 2, Downloaded from https://onlinelibrary.wiley.com/doi/10.1002/dep2.70071 by NICE, National Institute for Health and Care Excellence, Wiley Online Library on [14/04/2026]. See the Terms and Conditions (https://onlinelibrary.wiley.com/terms-and-conditions) on Wiley Online Library for rules of use; OA articles are governed by the applicable Creative Commons License

FIGURE 7 The outcrop, sedimentary structures, fossils and facies at Demirtaş. (A) Aerial view of the Permian–Triassic outcrop at Demirtaş, retrieved from the virtual model. (B) Formation boundary at Demirtaş, the head of the hammer stands between the Changhsingian wackestone of the Yüğlük Tepe Limestone and transitional oolites of the Sapadere Formation. (C) Rip-up clasts with carbonate cement just above yellow mudstones, Dienerian, Sapadere Formation, Taşlıca Member, TSD_7. (D) *Claraia clarae* (Emmrich, 1844) in yellow mudstones, Dienerian, Sapadere Formation, Taşlıca Member, BK-2024/89e. (E) *Claraia clarae* (Emmrich, 1844) in yellow mudstones, Dienerian, Sapadere Formation, Taşlıca Member, BK-2024/89a. (F) *Claraia aurita* (Hauer, 1850) and Kinneyia (wrinkle structures) in yellow mudstones, Dienerian, Sapadere Formation, Taşlıca Member, BK-2024/639. (G) Ooolitic grainstones with dolomite nucleus, which underlies the yellow mudstones, Griesbachian, Sapadere Formation, Beslengiler Limestone Member, TSD_1. (H) Laminar microbialites which overlies transitional oolites, Griesbachian, Sapadere Formation, Beslengiler Limestone Member, TSD_5. (I) *Earlandia* sp. in laminar microbialites which overlies transitional oolites, Griesbachian, Sapadere Formation, Beslengiler Limestone Member, TSD_5. (J) *Postcladella kalhori* (Brönnimann et al., 1972) in laminar microbialites Griesbachian, Sapadere Formation, Beslengiler Limestone Member, TSD_5. (K) A microgastropod in the transitional oolites, Changhsingian, Sapadere Formation, Beslengiler Limestone Member, TSD_4. (L) Packstone with *Gymnocodium* sp., bryozoa and bellerophontid gastropod, Changhsingian, Yüğlük Tepe Limestone.

is another extensive exposure of the Permian–Triassic transition (N36°28.7447, E032°14.7688; Alt. 173 m, Appendix 2-Figure 14), but the formation contact of the succession is not as well-exposed.

Generating the models for Demirtaş was cumbersome because of the dense woodland, making it difficult to fly the UAV and for the images from the UAV to be stitched when generating the model (Figure 7A). In addition, flying the UAV above the canopy hinders clear sight of the outcrops. Despite the dense vegetation, the Yüğlük Tepe Formation is well-exposed with dark grey packstones and wackestones filled with a diversity of fossils including crinoids, large bellerophontid gastropods, brachiopods, calcareous algae and foraminifera (Figure 7L; Appendix 2-Figure 16). There is no conodont biostratigraphy available from Demirtaş and the Changhsingian is inferred by the foraminifera *Paradagmarita monodi* (Groves et al., 2005; Özgül, 1985).

The Beslengiler Limestone Member starts with a thin oolite bed and consists of microbialite and oolite successions (Özgül, 1985; Figure 4). The transitional oolites at the base of the Sapadere Formation (Figure 7B,K) are poorly exposed. The overlying thick stromatolitic beds of the Sapadere Formation are well-exposed, forming a small cliff (Appendix 2-Figures 6 and 7). In the basal stromatolites, thin horizons of microgastropods and shelly debris can be observed. The thickness of the microbialite unit was measured 8–10 m in the type section of the Sapadere Formation, which is located ca. 2 km north-east of the studied section (Özgül, 1985). Subsequent studies reported different thicknesses for the 'microbialite unit' at the 'Demirtaş' section, that is, ~27.5 m in Groves et al. (2005), 20 m in Riccardi (2007) and ~18.5 m in Richoz (2006). We only measured ~9 m of microbialites (stromatolites and thrombolites) followed by 9.5 m of dominantly oolitic beds that also occasionally contain cross bedding (Figure 4). The differences between Groves et al. (2005) and other studies could be because the sections were measured at different locations, but the exact location was not given in Groves et al. (2005). The oolitic grainstones are, however, heavily recrystallized and it is difficult to discern sedimentological features in the field. The microbialites of the Beslengiler Limestone Member contains *Earlandia* sp. and *Postcladella kalhori*, which are overlain by oolites composed of ooids with dolomite crystals as nucleus (Figure 7G,H,I,J). The Taşlıca Member represents an abrupt transition to the siliciclastic–mudstone lithofacies, similar to the transition in the Kokarkuyu Formation in Çürük Dağ and the Werfen Formation in Italy. The Taşlıca Member is characterised by laminated, yellow-weathered mixed siliciclastic–carbonate beds with bedding planes exposing abundant, typical Lower Triassic bivalves, such as *Claraia clarae* (Emmrich, 1844), and *Neoschizodus* spp. (Figure 7D,E,F). The subsequent succession is poorly exposed as small outcrops within the woods.

4.3 | Öznurtepe Road and Creek

The Öznurtepe Road section (Figure 8A,B) is a road cut along the Küçüklü Köyü Yolu ~10 km north-east of Gazipaşa (Table 1). The Permian–Triassic transition at the Öznurtepe sections was first reported by Baud et al. (2009). When looking down into the valley of Sinad Creek from the Öznurtepe Road section, the Öznurtepe Creek section (Figure 8C,D) is visible on the western shore of the creek, where the weathering resisting Upper Permian limestones and Lower Triassic microbialites form a distinct cliff. The succession repeats itself due to faulting, and the creek and road sections do not connect along the strike of the beds. The Öznurtepe Creek section can be accessed by following an unpaved road into the creek valley that branches off Küçüklü Köyü Yolu ~2 km in the direction of Gazipaşa. The creek must be crossed to reach the western shore of Sinad Creek, where the Permian–Triassic transition is exposed at least twice due to faulting. In spring, the river level is typically high and potentially unsafe, but in autumn, the creek is mostly dried up. 3D outcrop models were created

20554877, 2026, 2, Downloaded from https://onlinelibrary.wiley.com/doi/10.1002/dep2.70071 by NICE, National Institute for Health and Care Excellence, Wiley Online Library on [14/04/2026]. See the Terms and Conditions (https://onlinelibrary.wiley.com/terms-and-conditions) on Wiley Online Library for rules of use; OA articles are governed by the applicable Creative Commons License

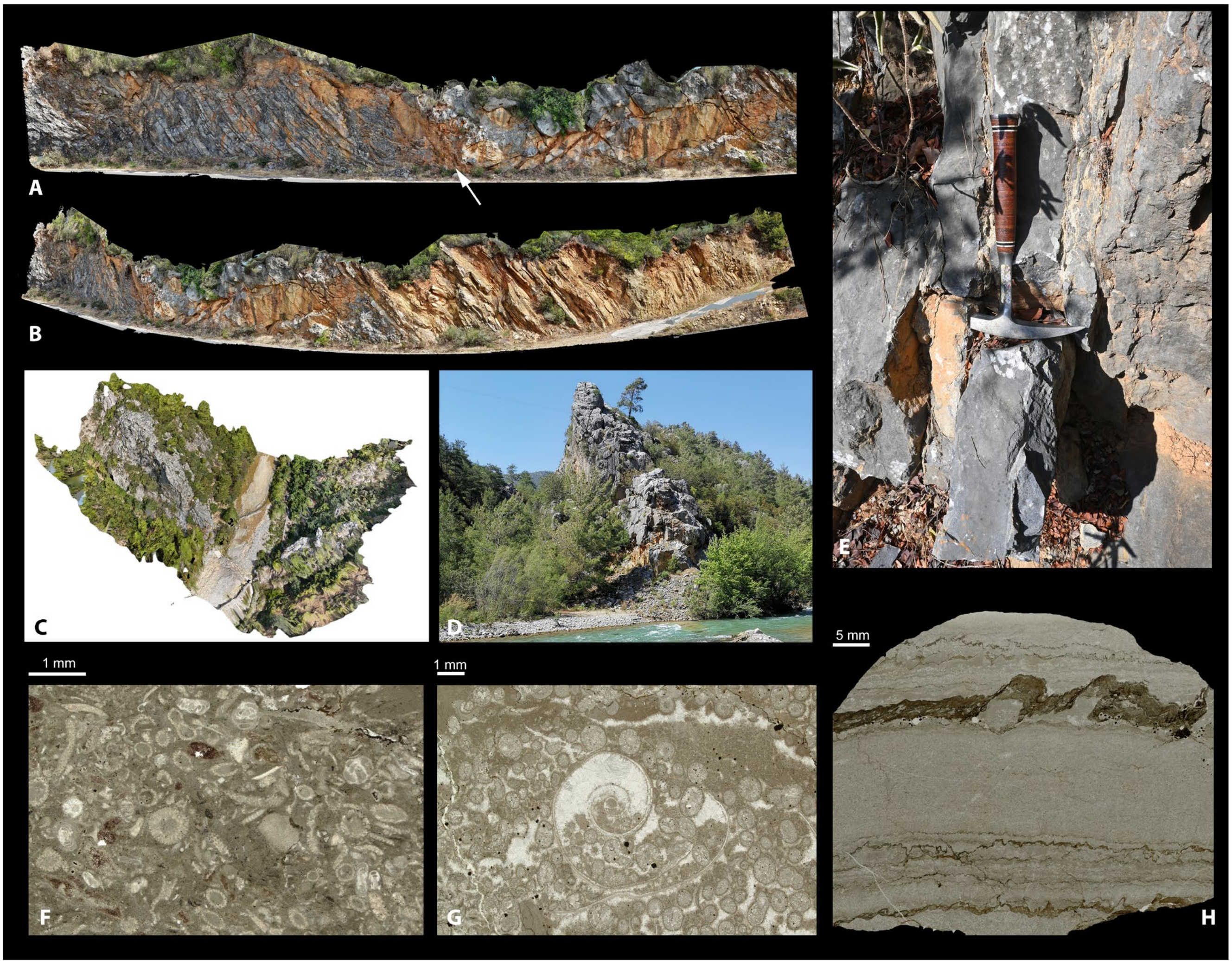

FIGURE 8 (A, B) Outcrop model of the Permian–Triassic outcrop at the Öznurtepe Road section. (A) Dark Upper Permian limestones of the Yüğlük Tepe Limestone (on the left), the formation boundary is obscured by heavy deformation (syncline and faults), white arrow indicates the uppermost bed of the Yüğlük Tepe Limestone that could be observed at the outcrop. The layers on the right side are the Griesbachian microbialites. (B) Continuation of the section, transition from the Griesbachian microbialites to yellow mudstone layers. (C) Outcrop model of the Permian–Triassic outcrop at the Öznurtepe Creek section. (D) Overview of the Öznurtepe Creek section, where the Early Triassic microbialites form a cliff. (E) Formation boundary between Yüğlük Tepe Limestone and Sapadere Formation, the hammer stands on the first transitional oolite bed of the Sapadere Formation. (F) *Permocalculus* sp. and foraminifera, Changhsingian, Yüğlük Tepe Limestone, TSO_1. (G) Transitional oolite with a bellerophontid gastropod, Changhsingian, Sapadere Formation, Beslengiler Limestone Member, TSO_3. (H) Microbialite layer with stylolites (dark bands), Griesbachian, Sapadere Formation, Beslengiler Limestone Member, TSO_4.

from the Öznurtepe Road section and the southern outcrop of the two repeating outcrops of the Öznurtepe Creek section. Whilst generating a digital 3D outcrop model from the road cut at Öznurtepe Road is rather straightforward, the vegetation at the Öznurtepe Creek affected the quality of the model by covering some parts of the section, but nevertheless, the formation boundary is visible in the model.

At the Öznurtepe Road and Creek sections (Figure 4), the Upper Permian Yüğlük Tepe Formation is composed of fossiliferous wackestone, which yield abundant fossils, for example, bellerophontids, crinoids and calcareous algae (Figure 8F; Appendix 3-Figures 5, 6, 22–26). At the Öznurtepe Road section, the Upper Permian Yüğlük Tepe Formation can be followed from lower to upper beds along the road, because the beds are highly tilted and almost vertical. At Öznurtepe Creek, the limestones of the Yüğlük Tepe Formation are overlain by a relatively thin (<10 cm thick) oolitic grainstone bed with similar characteristics (e.g. size, grade of recrystallization; Figure 8E,G) as other Permian–Triassic sections in the Taurides and other Tethyan deposits (Li et al., 2015). It is overlain by the Griesbachian stromatolitic and thrombolitic beds of the Beslengiler Member of the Sapadere Formation. The contact between the oolitic grainstone and the first

20554877, 2026, 2, Downloaded from https://onlinelibrary.wiley.com/doi/10.1002/dep2.70071 by NICE, National Institute for Health and Care Excellence, Wiley Online Library on [14/04/2026]. See the Terms and Conditions (https://onlinelibrary.wiley.com/terms-and-conditions) on Wiley Online Library for rules of use; OA articles are governed by the applicable Creative Commons License

microbialite bed had been dissolved (Kershaw in Baud et al., 2009, figs. 40, 42).

At Öznurtepe Road, the Yüğlük Tepe/Sapadere formation boundary is obscured by calcite crystals that have formed in a zone of severe tectonic deformation and folding (Figure 8A). When following the road towards Gazipaşa (southwards), the thick microbialitic beds of the Beslengiler Member of the Sapadere Formation are also exposed at Öznurtepe Road above the syncline hinge zone (Figure 8B). In contrast to Çürük Dağ where several thrombolitic beds and domal stromatolites can be observed, only one <50 cm thick domal stromatolite bed was identified at Öznurtepe by Kershaw et al. (2012), and the microbialites mainly consist of planar stromatolites (Figure 8H). In the microbialites, microfossils (foraminifera, ostracods, gastropods) have been found in low abundances and diversity (Foster et al., 2019). Above the microbialites, thick oolitic beds are formed in the Early Triassic, with ooids with a diameter up to 1 mm (Appendix 3-Figure 32). They are overlain by thinly bedded yellow-weathered mixed siliciclastic-carbonates of the Taşlıca Member, that exposes beds with ripple marks (Appendix 3-Figure 18). In addition, the Taşlıca Member hosts the first Triassic macrofossils including the cosmopolitan bivalves *Claraia*, *Unionites*? and *Neoschizodus* (Appendix 3-Figures 13–16). In the Öznurtepe Creek section, the yellow weathering mudstones of the Taşlıca Member were metamorphosed into slates with crenulation folds (Appendix 3-Figure 33; Bozkaya & Yalçın, 2005).

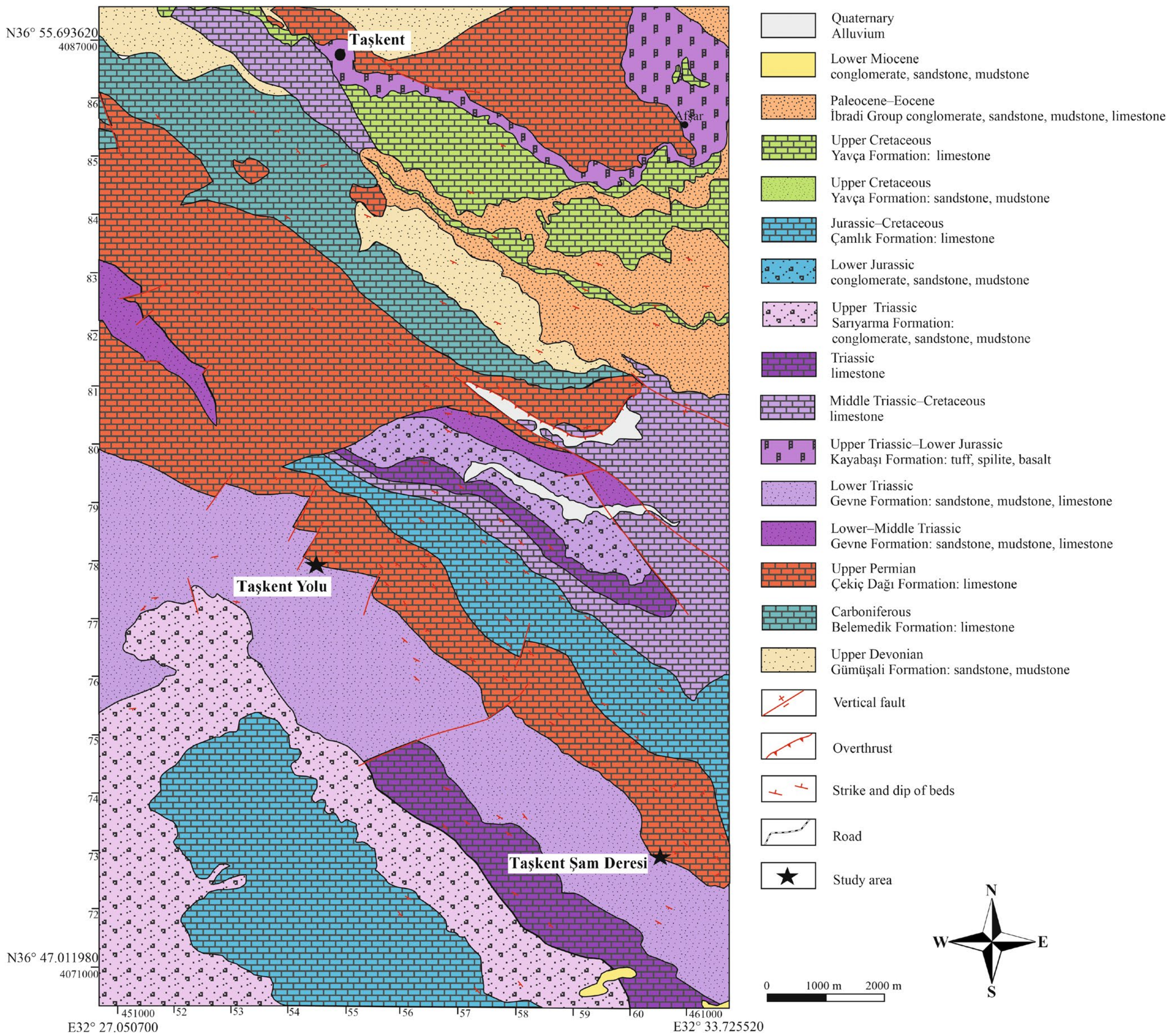

FIGURE 9 Geological map of the region around the study area in Taşkent (modified after MTA 1:25.000 scale maps). Coordinates are given in Universal Transverse Mercator (Zone 36S) and in World Geodetic System (WGS1984).

20554877, 2026, 2, Downloaded from https://onlinelibrary.wiley.com/doi/10.1002/dep2.70071 by NICE, National Institute for Health and Care Excellence, Wiley Online Library on [14/04/2026]. See the Terms and Conditions (https://onlinelibrary.wiley.com/terms-and-conditions) on Wiley Online Library for rules of use; OA articles are governed by the applicable Creative Commons License

4.4 | Taşkent

The Permian–Triassic transition at Taşkent region can be followed for kilometres along strike in this area (Figure 9). Numerous authors have reported Permian–Triassic investigations at the 'Taşkent section' (Altıner et al., 2021; Baud et al., 2005; Payne et al., 2007), but they measured it at different locations. Calling several sections by a single name might cause confusion; therefore, we here name the sections separately. After reviewing the available information, most previous studies correspond to the Taşkent Yolu section (Baud et al., 2005; Payne et al., 2007). Three additional exposures at Taşkent Yolu Hill, Taşkent Şam Deresi, and Taşkent Şam Deresi Hill were also investigated, but nothing appears to be published on these thus far. Taşkent Şam Deresi is ca. 700 m south of the GPS point given for the DT section in Altıner et al. (2021; N36°48.335, E032°33.258). However, the sections previously reported as DT and TCX in Altıner et al. (2021, 2024) are actually near the Taşkent Yolu section (D. Altıner pers. comm. BK), rather than being near to the Taşkent Şam Deresi section. Below the oolitic grainstones (transitional oolites) marking the formation boundary in Taşkent, and 50 m of the Changhsingian were measured by Altıner et al. (2021).

4.4.1 | Taşkent Yolu

The Taşkent Yolu (Road) section is exposed ca. 9 km south of the Taşkent district, Konya (Figure 9, Table 1). The exposure described here is on the northern side of the road and was excavated to widen the road in 2024 when the pictures were taken for the outcrop models (Figure 10D,E,F). The studied section is ca. 0.6 km south of the GPS coordinates given by Baud et al. (2005) and Payne et al. (2007) but is the same section studied by those authors, as was also indicated by markings on the Taşkent Yolu section before the new road construction. The GPS location given by Baud et al. (2005) and Payne et al. (2007) is herein named Taşkent Yolu Hill to differentiate it from the Taşkent Yolu section.

Starting from the Taşkent Yolu Hill section, the Çekiç Dağı Formation yields limestone facies with large calcareous algae (1 cm in diameter) *Permocalculus anatoliensis* (Güvenç, 1966) (Appendix 4-Figure 1) and large gastropods (Appendix 4-Figures 2–4). At Taşkent Yolu, the skeletal carbonates of the Çekiç Dağı Formation are overlain by oolitic grainstones and microbialites of the İspatlı Member of the Gevne Formation. A depositional gap and pressure dissolution (stylolitic contact) have been interpreted at the Permian/Triassic boundary based on the truncation on top of the oolite bed at Taşkent (Payne et al., 2007; Ünal et al., 2003). Baud et al. (2005) reported pressure dissolution at the contact between nodular limestone and the uppermost Changhsingian oolite bed and the overlying Griesbachian stromatolite at Taşkent. As in other sections, the carbonate succession is overlain by siliciclastic mudstones. The yellow mudstones of the İspatlı Member of the Gevne Formation at this locality yield an undescribed myophoricardiid bivalve genus and the cosmopolitan bivalves *Neoschizodus* and *Eumorphotis* (Figure 11B,C). The yellow siliciclastic-carbonate beds also bear an unidentified ammonoid in a gastropod-oolite packstone (Figure 11D). Different from the sections in Antalya, large oncolites (Figure 11A; Appendix 4-Figures 7 and 8) and oolites with microgastropods are deposited above the yellow-weathered siliciclastic–carbonate beds, but could be part of a juxtaposed block.

Towards younger beds on the southern side of the road, oolitic grainstone deposits composed of microgastropods and oolitic rip-up clasts are cropping out (Appendix 4-Figures 11–15). These are overlain by green–grey siliciclastics with abundant microgastropods. On top of that are reddish siliciclastics with ripple marks, gutter casts and rip-up clasts (Figure 12E–F, Appendix 4-Figures 16–18). The reddish silicilastics also have Kinneyia (Figure 12G), a sedimentary structure also known as wrinkle marks that has been interpreted as being formed by microbial mats (e.g. Pruss et al., 2004), but might also be formed by physical processes, such as earthquakes (Herminghaus et al., 2016; Pratt, 2021). These siliciclastics are overlain by light grey calcareous mudstone, having a vermiform appearance (Appendix 4-Figures 19, 20 and 24). Thin sections reveal that the vermiform appearance is a result of micro pressure dissolution (Figure 12B). These grey limestones intercalate with the green to reddish mudstones and in the upper part of the succession (Appendix 4-Figure 21). The grey limestones with micro pressure dissolution structures cropping out ca. 1.4 km south-west of the Permian/Triassic boundary, and yield *Tirolites cassianus* (Quenstedt, 1849, Figure 12C), indicating the Spathian substage (e.g. Broglio Loriga et al., 1990). Around this outcrop, it is also possible to find yellow mudstones with *Ladinaticella costata* (Münster, 1841) and *Rhizocorallium* isp. and the gastropod oolite bed, characterised by dominant and moderately diverse gastropod fauna (Figure 12A,D; Appendix 4-Figure 25).

4.4.2 | Taşkent Şam Deresi

The Taşkent Şam Deresi (Creek) section (Figure 10A,B,G, Table 1) is located along the road parallel to Şam Deresi.

20554877, 2026, 2, Downloaded from https://onlinelibrary.wiley.com/doi/10.1002/dep2.70071 by NICE, National Institute for Health and Care Excellence, Wiley Online Library on [14/04/2026]. See the Terms and Conditions (https://onlinelibrary.wiley.com/terms-and-conditions) on Wiley Online Library for rules of use; OA articles are governed by the applicable Creative Commons License

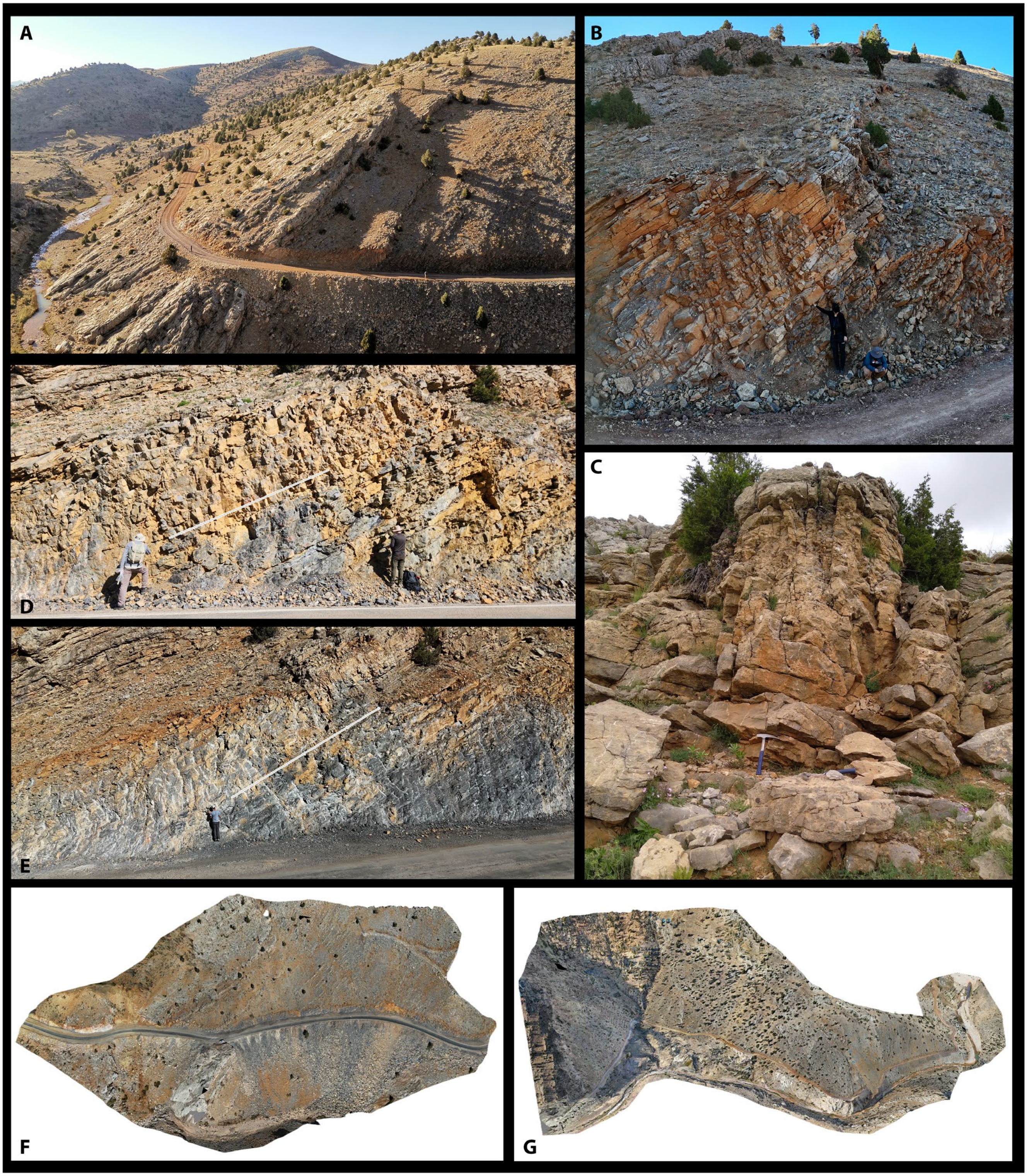

FIGURE 10 (A) Overview Taşkent Şam Deresi section, where Upper Permian limestones of the Çekiç Dağı Formation are overlain by Lower Triassic Gevne Formation. (B) Formation boundary between the Çekiç Dağı Formation and the Triassic Gevne Formation, pointed by a person. (C) Taşkent Şam Deresi Hill section, the hammer stands at the formation boundary. (D) Overview of the Permian–Triassic transition at the Taşkent Yolu section before the road construction, the line indicates the formation boundary between the Çekiç Dağı Formation and the Gevne Formation. (E) The Permian–Triassic transition at the Taşkent Yolu section after the road construction. (F) 3D outcrop model of the Permian Triassic outcrop at Taşkent Yolu section. (G) 3D outcrop model of the Permian-Triassic outcrop at Taşkent Şam Deresi section.

20554877, 2026, 2, Downloaded from https://onlinelibrary.wiley.com/doi/10.1002/dep2.70071 by NICE, National Institute for Health and Care Excellence, Wiley Online Library on [14/04/2026]. See the Terms and Conditions (https://onlinelibrary.wiley.com/terms-and-conditions) on Wiley Online Library for rules of use; OA articles are governed by the applicable Creative Commons License

The Permian limestone–mudstone alternation continues and reaches up to a couple of hundred metres, but the position of the Wuchiapingian/Changhsingian stage boundary is uncertain in the succession. The Upper Permian Çekiç Dağı Formation yields large gastropods, algae, crinoids, echinoids, bryozoans and brachiopods including *Comelicania*, *Orthothetina* and *Spinomarginifera* (Figure 11K,L,M,N, Appendix 4-Figures 35 and 36). As in the Taşkent Yolu section, the skeletal carbonates are overlain first by the oolitic grainstones of the transitional oolites and microbialites, then by large oncolites (Figure 11G,H,I,J).

Higher in the section, the carbonate succession of the İspatlı Member of the Gevne Formation terminates

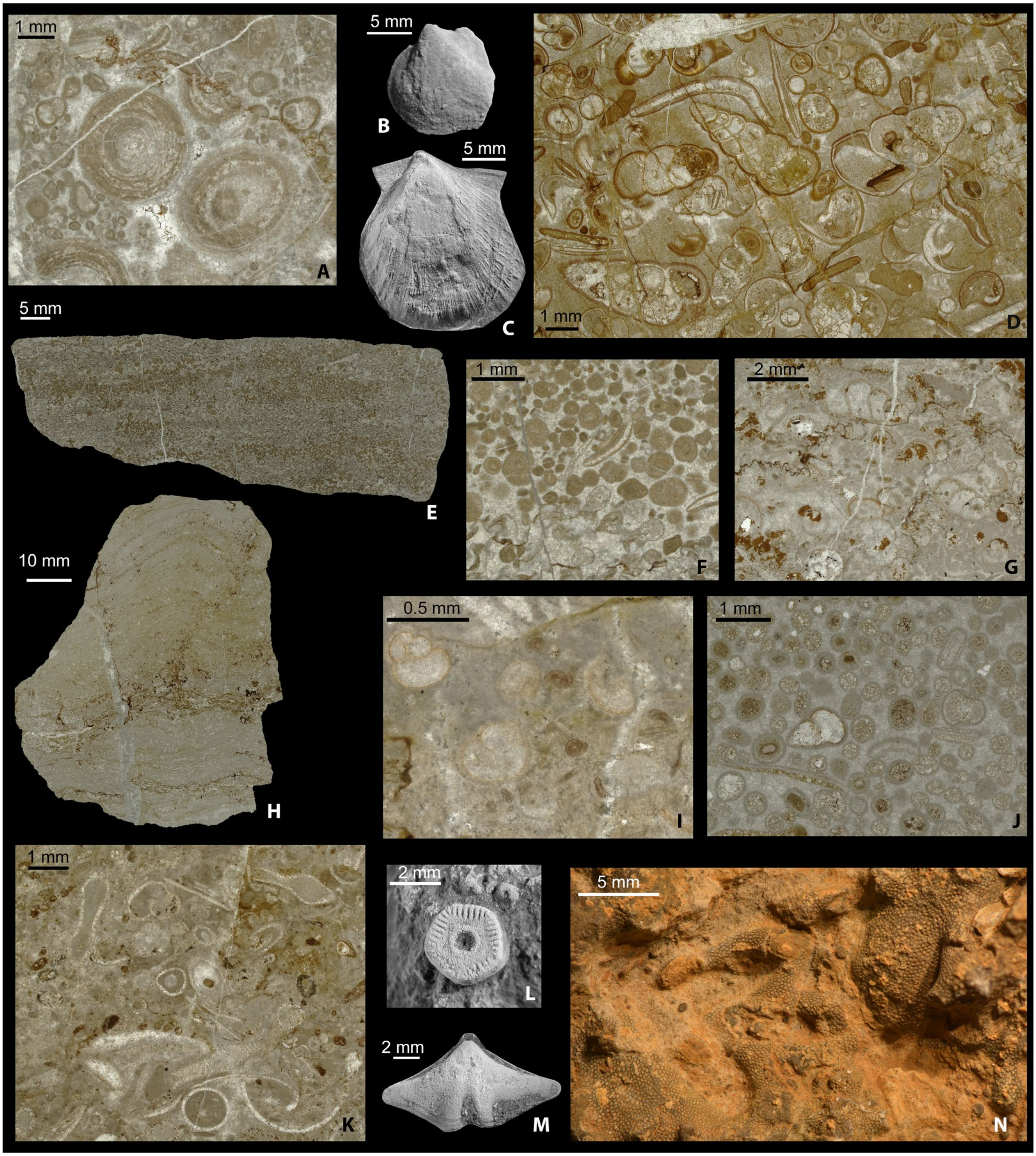

FIGURE 11 Legend on next page.

20554877, 2026, 2, Downloaded from https://onlinelibrary.wiley.com/doi/10.1002/dep2.70071 by NICE, National Institute for Health and Care Excellence, Wiley Online Library on [14/04/2026]. See the Terms and Conditions (https://onlinelibrary.wiley.com/terms-and-conditions) on Wiley Online Library for rules of use; OA articles are governed by the applicable Creative Commons License

FIGURE 11 Sedimentary structures, fossils and facies at Taşkent. (A) Thin section of oncolites, Dienerian, Gevne Formation, TSTB_2, Taşkent Yolu section. (B) *Neoschizodus* aff. *praeorbicularis* (Bittner, 1901), Dienerian, Gevne Formation, BK-2024/625, Taşkent Yolu section. (C) *Eumorphotis multiformis* (Bittner, 1899), Dienerian, Gevne Formation, BK-2024/159, Taşkent Yolu section. (D) Thin section of ammonoid bearing gastropod oolite found in the yellow siliciclastics, Dienerian, Gevne Formation, TSTB_1, Taşkent Yolu section. (E) Thin section of oolitic grainstone with dark stripes, Dienerian, Gevne Formation, TSTDT_5, Taşkent Şam Deresi section. (F) Close up of oolitic grainstone with dark stripes, Dienerian, Gevne Formation, TSTDT_5, Taşkent Şam Deresi section. (G) *Coelostylina* sp. in domal thrombolites above the laminar microbialite layer, Griesbachian, Gevne Formation, TSTDT_3, Taşkent Şam Deresi section. (H) Thrombolite just above the transitional oolites, Griesbachian, Gevne Formation, TSTDT_1, Taşkent Şam Deresi section. (I) Microgastropods, *Earlandia* sp. and *Postcladella kalhori* (Brönnimann et al., 1972) in laminar microbialites just above the thrombolite layer, Griesbachian, Gevne Formation, TSTDT_2, Taşkent Şam Deresi section. (J) Transitional oolites, with juvenile bellerophontid and *Coelostylina* sp., uppermost Changhsingian, Gevne Formation, TSTDT_0, Taşkent Şam Deresi section. (K) Packstone with *Permocalculus* sp., gastropods and bivalves, Changhsingian, Çekiç Dağı Formation, TSTDT_8, Taşkent Şam Deresi section. (L) Crinoid columnal, Changhsingian, Çekiç Dağı Formation, BK-2024/117, Taşkent Şam Deresi section. (M) *Comelicania haueri* (Stache, 1878), Changhsingian, Çekiç Dağı Formation, BK-2024/116, Taşkent Şam Deresi section. (N) Bryozoans, Changhsingian, Çekiç Dağı Formation, BK-2024/711, Taşkent Şam Deresi section.

with an oolitic grainstone bed showing dark stripes (Appendix 4-Figures 41–43). The dark stripes appear to originate from the intercalation of aragonitic ooids and calcitic grains (Figure 11E,F). These oolitic grainstones also yield medium-sized bivalves, possibly myophorids. The yellow-weathered siliciclastic-carbonate beds are not well-exposed in the section, and due to many faults, the succession appears to be repeated, making it difficult to measure; however, the subsequent unit of poorly cemented, green and reddish siliciclastics is well-exposed along the road. There are abundant *Neoschizodus* and *Eumorphotis* on the bedding surfaces of the siltstones in this unit. They also yield a horizon with tubular structures composed of mudstone (Figure 12J, Appendix 4-Figures 45–47), which are either rip-up clasts or possibly redeposited burrow moulds. Further along the section, the reddish mudstones are overlain by yellow mudstone deposits with large burrows (*Rhizocorallium* isp. Appendix 4-Figure 48). The gastropod *Ladinaticella costata* (Münster, 1841) and large *Bakevellia* sp. reach up to 4 cm (Appendix 4-Figures 49 and 50). Large *Bakevellia* species and *Ladinaticella costata* are also characteristic of the Spathian Val Badia Member of the Werfen Formation in the Dolomites, Italy (Neri & Posenato, 1985).

In all studied sections of the Antalya and Aladağ Nappes, the Permian–Triassic transitional deposits start with the carbonate beds classified as wackestones/packstones and continue with oolite, microbialite, stromatolites, then with yellow coloured Dienerian mudstones. Although some greenish mudstones, possibly from the Smithian, were found in Çürük Dağ, the reddish silicilastics of the Olenekian are only exposed in Taşkent (Figure 12E,G), which are overlain and intercalated with *Tirolites* bearing grey coloured mudstones, indicating the Smithian/Spathian boundary (Figure 12B,C). Hence, environmental and community evolution can be tracked for a much longer interval in Taşkent.

5 | ENVIRONMENTAL EVOLUTION ACROSS THE PERMIAN–TRIASSIC IN THE ANTALYA AND ALADAĞ NAPPES AND THEIR CORRELATION WITH OTHER SECTIONS

The lithofacies of the Permian Pamucak (Çürük Dağ), Yüğlük Tepe (Demirtaş, Öznurtepe), and Çekiç Dağı (Taşkent) formations are similar to shallow marine, pre-extinction, carbonate platforms successions known from across the Palaeo- and Neotethys oceans (e.g. Great Bank of Guizhou: Lehrmann et al., 2003, and Transcaucasian–NW Iranian region: e.g. Gliwa et al., 2020), in that they are skeletal limestones dominated by calcareous algae, fusulinid foraminifera, large gastropods, crinoids, rugose corals, bryozoans and brachiopods (Altıner et al., 2000; Ünal et al., 2003; Figures 5H,I,J,K,L,M, 7L, 8F and 11K,L,M,N). In addition, the stromatolite, thrombolite and dolomitized oolitic lithofacies at the base of the post-extinction (mostly Griesbachian) Kokarkuyu (Çürük Dağ), Sapadere (Demirtaş, Öznurtepe) and Gevne (Taşkent) formations are also consistent with shallow, post-extinction carbonate platform successions from across the Palaeo- and Neotethys oceans.

The pre-extinction Permian formations in the Antalya and Aladağ nappes contain calcareous algae including the red algae *Gymnocodium* and *Permocalculus* at Demirtaş, Öznurtepe and Çürük Dağ, indicating a shallow water environment on the shelf in the photic zone (ca. 0–200 m depth, Flügel & Munnecke, 2010). At Çürük Dağ, the Permian Pamucak Formation terminates with nodular limestones, before the transitional oolites of the Kokarkuyu Formation. It is unsure whether the nodular limestones and intercalated thin layers of mudstones were formed as a result of post-depositional processes (such as pressure dissolution), or reflect the synsedimentary

20554877, 2026, 2, Downloaded from https://onlinelibrary.wiley.com/doi/10.1002/dep2.70071 by NICE, National Institute for Health and Care Excellence, Wiley Online Library on [14/04/2026]. See the Terms and Conditions (https://onlinelibrary.wiley.com/terms-and-conditions) on Wiley Online Library for rules of use; OA articles are governed by the applicable Creative Commons License

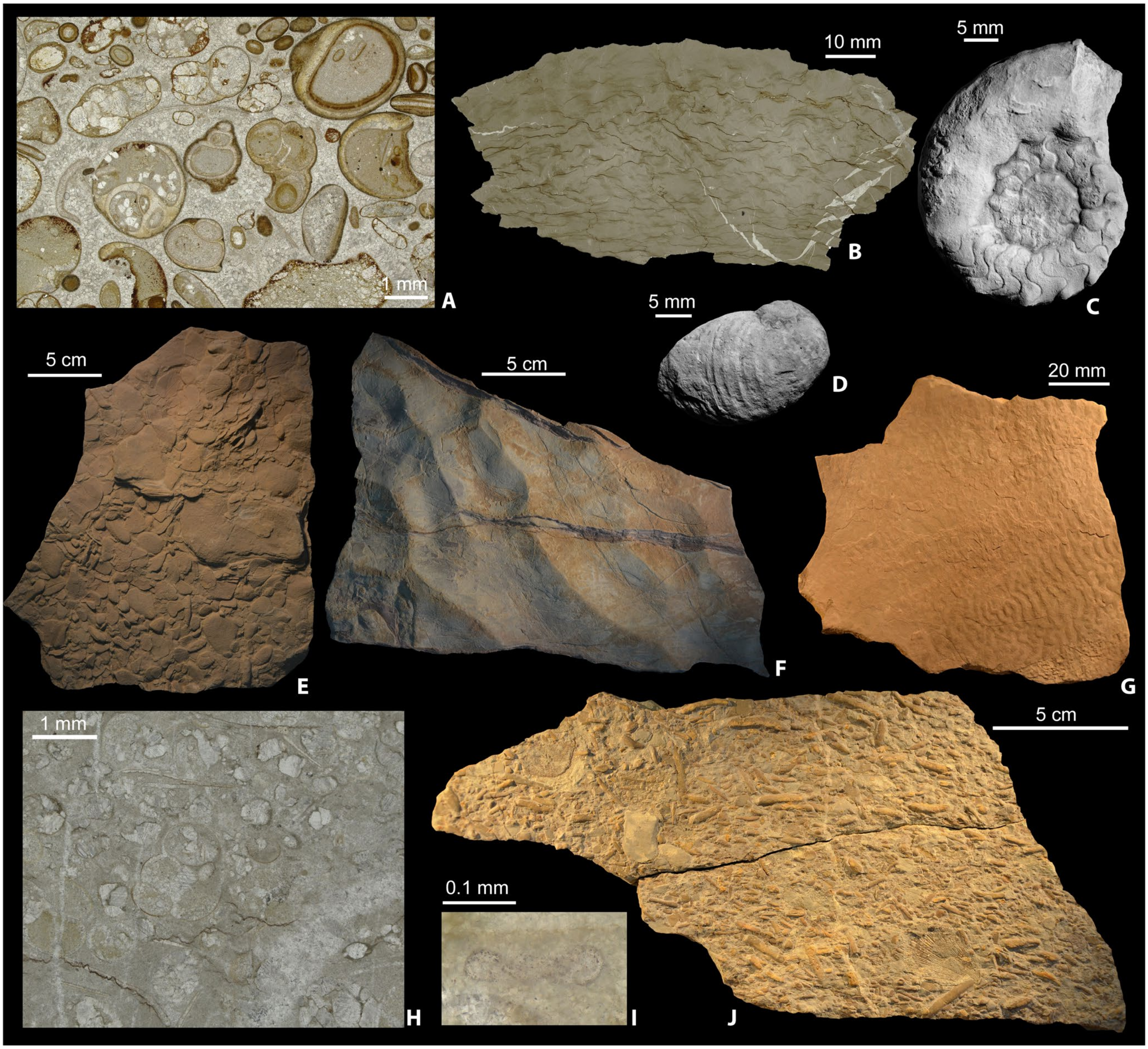

FIGURE 12 Sedimentary structures, fossils and facies at Taşkent. (A) Gastropod oolite, Spathian, Gevne Formation, TSTBAm_1, Taşkent Yolu section. (B) Pressure dissolution (dark lines) in the thin section of grey limestone with *Tirolites cassianus*, Spathian, Gevne Formation, TSTBAm_2, Taşkent Yolu section. (C) *Tirolites cassianus* (Quenstedt, 1849), Spathian, Gevne Formation, BK-2024/174, Taşkent Yolu section. (D) *Ladinaticella costata* (Münster, 1841) in yellow mudstones, Spathian, Gevne Formation, BK-2024/676, Taşkent Şam Deresi section. (E) Flat pebbles in reddish siliciclastics, Smithian, Gevne Formation, BK-2024/722, Taşkent Şam Deresi section. (F) Ripple marks in reddish siliciclastics, Smithian, Gevne Formation, BK-2024/709, Taşkent Şam Deresi section. (G) Kinneyia (wrinkle structures) on reddish siliciclastics, Smithian, Gevne Formation, BK-2024/163, Taşkent Yolu section. (H) Microgastropod in carbonate mudstones, below greenish siliciclastic mudstones, Dienerian, Gevne Formation, TSTDT_4, Taşkent Şam Deresi section. (I) *Postcladella kalhori* (Brönnimann et al., 1972) in carbonate mudstones, below greenish siliciclastic mudstones, Dienerian, Gevne Formation, TSTDT_4, Taşkent Şam Deresi section. (J) Tubular structures (rip-up clasts or redeposited burrow moulds) and *Eumorphotis* sp. in greenish mudstone, Smithian, Gevne Formation, BK-2024/138, Taşkent Şam Deresi section.

depositional regime shifts from carbonate dominance to siliciclastic dominance (due to variations in carbonate to clay input), or might be formed as a result of heavy bioturbation (e.g. Kahsnitz & Willems, 2019). The presence of *Spinomarginifera* and the high mud content in limestones suggest soft ground in the uppermost Permian. The spines of productid brachiopods are thought to serve for anchoring in soft sediments (Grant, 1968; Leighton, 2000). The carbonate rosettes found in the Permian of Çürük Dağ have been interpreted as possible pseudomorphs of ikaite (glendonites), and if so could be a possible indicator of cold-water influence (Angiolini et al., 2007). However,

20554877, 2026, 2, Downloaded from https://onlinelibrary.wiley.com/doi/10.1002/dep2.70071 by NICE, National Institute for Health and Care Excellence, Wiley Online Library on [14/04/2026]. See the Terms and Conditions (https://onlinelibrary.wiley.com/terms-and-conditions) on Wiley Online Library for rules of use; OA articles are governed by the applicable Creative Commons License

ikaite forms up to 35°C, hence, it may indicate high alkalinity rather than cold water (Rogov et al., 2023). The rosettes are also present in lower horizons in the Permian Çürük Dağ section (Appendix 6), in the Late Permian of Hadim (Konya) and Hazro (Diyarbakır). Similar clusters, identified as nodular celestites, were found in the Permian of Oman and China (Beckert et al., 2016; Yan & Carlson, 2003).

Following the depositional model that Ünal et al. (2003) suggested for the Permian–Triassic transition in the Aladağ Nappe in the Central Taurides, a shallowing upward trend can be interpreted until the transitional oolites for all sections. Above, there were oscillations in water depth, first a slight deepening indicated by slightly offshore microbialites (recorded as being formed by layered cyanobacterial, benthic mats; Heindel et al., 2018) and then shallowing indicated by near shore oolites and clastic deposits with ripple marks, the latter suggesting deposition in a setting above wave base. The dominance of anachronistic lithofacies as oolite deposits, microbialites and calcite crystal fans reflects deposition when sea water was probably super-saturated with respect to calcium carbonate (Foster et al., 2019; Kershaw et al., 2011; Pruss et al., 2006) and a disruption of the carbon cycle as a result of extinction or decline of biomass of organisms with skeletal carbonate (Groves et al. 2005). Oolite deposition has been observed in many other sections across the Permian–Triassic transition in the Tethys (e.g. Haas et al., 2007; Li et al., 2015).

It is also noteworthy that the timing of the carbon isotope excursion is different between the three sections. At Taşkent, the isotope excursion onset is 40 cm below the transitional oolites (onset of extinction), at Demirtaş ~250 cm below the transitional oolites and at Çürük Dağ, at the base of the transitional oolites (Riccardi, 2007; Richoz, 2006). A similar diachronous pattern in the carbon isotope excursion has also been observed for the lowermost oolitic beds of the Tesero Member in the Dolomites, Italy (Kraus et al., 2009). This suggests that the transitional oolitic beds are diachronous, and the transitional oolites at Demirtaş (Sapadere Formation) is stratigraphically younger than at the Taşkent (Gevne Formation) and Çürük Dağ sections (Kokarkuyu Formation). The stromatolites and microbialites in the studied sections also coincide with the lack or low abundance of microbial grazers, as also suggested by few occurrences of gastropods in the thin sections. The proliferation of microbialites might indicate that mat-inhibitors (such as grazers) were not present at microbialite suppressing abundances (Schubert & Bottjer, 1992), or alternatively a lack or suppression of competitors (such as macroalgae, sponges or other bacteria) (Foster et al., 2020; Mata & Bottjer, 2012). Potential high salinity episodes were suggested based on the biomarkers found in the microbial mats (Heindel et al., 2018). The stromatolites could also indicate high salinity in the Griesbachian, as recent marine stromatolites are formed in high salinity marine environments (e.g. Shark Bay in Australia), but they are formed also in normal saline environments. If correct, high salinity, in addition to high temperatures (Gliwa et al., 2022), may explain harsh conditions for life and suppressing of grazers or competitors of microbial mat producers. Widely accepted anoxia (Sperling et al., 2022), on the other hand, was not present in the studied sections and cannot be considered a major agent for proliferation of microbialites or the suppression of other organisms (Frank et al., 2025).

The second major sedimentological shift occurs in the late Griesbachian–Dienerian, where the carbonate succession shifts to a mixed siliciclastic–carbonate succession characteristic of the homoclinal carbonate ramps from central Europe during the Early Triassic (e.g. Werfen Formation, Italy: Broglio Loriga et al., 1983; Servino Formation, Italy: Foster et al., 2018; or Aggtelek Karst, Hungary: Hips, 1998, Foster et al., 2015). The change from carbonate platform facies to a mixed siliciclastic–carbonate homoclinal ramp facies (Appendix 8) marks the extinction of the platform forming calcareous algae and indicates an increase in sediment supply, which might be associated with increased physical weathering rates due to increased temperatures or declined plant biomass (Algeo & Twitchett, 2010; Xu et al., 2025), and rifting during the opening of the Neotethys (Şahin & Altıner, 2019). From the Dienerian onwards, storm-induced rip-up clasts, flat pebbles and tempestites in Çürük Dağ, Öznurtepe, Demirtaş and Taşkent indicate deposition above storm-weather wave base (e.g. Hips, 1998; Török, 1998; Wignall & Twittchett, 1999). Some Dienerian rocks in Çürük Dağ contain bivalve external moulds, infilled with differently coloured sediments, indicating occasional subaqueous shell dissolution and a depositional hiatus.

During the Smithian, in northern Italy, Austria, Croatia and both the Aggtelek Karst and Balaton Highlands in Hungary, the mixed carbonate–siliciclastic successions are represented by reddish siltstones and sandstones interpreted to represent a 'terrigenous event', often referred to as the Campil Event (Aljinović, 1995; Broglio Loriga et al., 1990; Foster et al., 2018; Hips, 1998; Hofmann et al., 2015; Posenato, 2008; Twitchett & Wignall, 1996). Part of the İspatlı Member of the Gevne Formation at the Taşkent sections is also a red coloured terrigenous unit. It contains *Eumorphotis reticulata* (Richthofen, 1860) and *Costatoria subrotunda* (Bittner, 1901), and is characterised by a negative isotope excursion (Richoz, 2006, fig. 5.13) that are characteristic to Smithian beds of the Werfen Formation (Broglio Loriga & Mirabella, 1986; Broglio

20554877, 2026, 2, Downloaded from https://onlinelibrary.wiley.com/doi/10.1002/dep2.70071 by NICE, National Institute for Health and Care Excellence, Wiley Online Library on [14/04/2026]. See the Terms and Conditions (https://onlinelibrary.wiley.com/terms-and-conditions) on Wiley Online Library for rules of use; OA articles are governed by the applicable Creative Commons License

20554877, 2026, 2, Downloaded from https://onlinelibrary.wiley.com/doi/10.1002/dep2.70071 by NICE, National Institute for Health and Care Excellence, Wiley Online Library on [14/04/2026]. See the Terms and Conditions (https://onlinelibrary.wiley.com/terms-and-conditions) on Wiley Online Library for rules of use; OA articles are governed by the applicable Creative Commons License

Loriga & Posenato, 1986; Twitchett & Wignall, 1996). This suggests that the Campil Event is also represented in deposits in Türkiye and that the Taşkent successions can be correlated to successions in Europe. In addition, the younger abrupt positive isotope excursion (Richoz, 2006, fig. 5.13) and shift to limestones and marls are equivalent to the lower Spathian Val Badia Member of the Werfen Formation in Italy (Broglio Loriga et al., 1983) and other units across central Europe (e.g. Szin Marl Formation in Hungary: Foster et al., 2015; Hips, 1998; 'Myophoria beds', Servino Formation, Italy: Foster et al., 2018) both in terms of lithology and fossil content, that is, the diagnostic *Tirolites cassianus* (Quenstedt, 1849) and *Ladinaticella costata* (Münster, 1841). These similarities suggest that the environmental changes across the Smithian–Spathian transition can be directly correlated between central European sections and sections in Türkiye.

6 | ADHERING TO FAIR PRINCIPLES

Whilst reviewing the pre-existing data from the Permian–Triassic successions in Türkiye, it became clear that an improvement in technology is not the only way that earth scientists can better adhere to the FAIR principles (Findable, Accessible, Interoperable, Reusable; Wilkinson et al., 2016). In some publications, the data are only described, but the original raw data are not made publicly available; hence, it is not available for use by subsequent researchers. Keeping the raw data confidential prevents comparing the results with replicated data (in the case of geochemical data), or testability (for instance, identification of fossil specimens) and might result in subsequent loss of the original data. There are also examples where the raw data is shown in a figure (such as a range chart; Marcoux & Baud, 1988; or time-series curve: Riccardi, 2007; or stratigraphic column: Altıner et al., 2021; Varol et al., 2011), but the data are not in an accessible format (such as a data table with exact measurements and sampling points along the section), so the data may not be integrated into new analyses without potential errors in their true position along the log.

Another issue arises when geochemical data is included only as calculated ratios or proxies, such as Mg/Ca or Ce anomalies, rather than the original elemental concentrations, as methods can evolve, inhibiting the comparison of modern studies with the published record. Good examples are Loope et al. (2013) and Frank et al. (2025), who used different methods to calculate Ce anomalies but provided original element concentrations, enabling a recalculation and comparison of the proxy between the Demirtaş (Loope et al., 2013), Çürük Dağ and Öznurtepe sections (Frank et al., 2025) using the same method. Hence, we recommend providing the complete datasets used in a study in a usable tabular form, which enables reproducibility as well as continued use of the previously produced data, even if methods evolve.

In the case of palaeontological studies, previous studies provided names in range charts (e.g. Jenny in Marcoux et al., 1986; Jenny in Richoz, 2006), but taxonomic names differ among publications even in the publications with the same author published in different years, generally as a result of taxonomic revisions. In the absence of figures of identified specimens, the identifications cannot be verified, and in the long term, the different names used for the same taxon create an artificial inflation of diversity. Sometimes, authors mention key index fossils that are also not figured, such as *Claraia* (e.g. Baud et al., 2009; Özgül, 1985). To the best of our knowledge, we provide the first image of *Claraia* from the studied sections (Figure 7D,E,F). We recommend that authors provide images of fossils, even if they are poorly preserved. This will help to better assess the original community composition, infer changes in biodiversity, identify the patterns of extinction more accurately and confirm identifications of fossils that are used to make biostratigraphic age assignments. A good example from Türkiye is Angiolini et al. (2007), who despite focusing on brachiopods showed images of foraminifera, algae and conodonts mentioned in the text. Providing images is important not only for the verification of taxonomic identifications and preventing over- or underestimations of diversity, but also for recording additional data (e.g. body size) of fossils to assess an ecological response.

ACKNOWLEDGEMENTS

We thank Saliha Dündar (TPAO) and Jörn Peckmann (University of Hamburg) for assisting us with fieldwork and John Payne (Stanford University) for assisting us remotely with fieldwork and sharing their wealth of information on the sections they have visited. Martin Nose (SNSB-BSPG) and Birgit Leipner-Mata (FAU Erlangen-Nürnberg) are acknowledged for helping prepare thin sections. Crispin Little and Paul Wignall (University of Leeds) are acknowledged for the discussion on the tubular structures found in the Lower Triassic at Taşkent. Bingqian Wang, Xin Chen, Jianhua Chen and Hanting Zhong are thanked for their help in review and upload the 3D models in Outcrop3D. BK, SZB, ABF, MAGC and WJF were funded by Deutsche Forschungsgemeinschaft (project no. FO1297/1-1). BK further received funding from NERC (NE/X012859/1; NE/X015025/1) for some of the field trips. MG funded by MTA (Project no 2024-08-16-02-1). XW received funding from the National Natural Science Foundation of China (NSFC) project no 42293291 and 42102143. We thank two anonymous reviewers, Thomas

Algeo and the editor Elias Samankassou for their feedback on the initial draft of the manuscript.

DATA AVAILABILITY STATEMENT

All datasets, including the outcrop models and supplementary appendices, are openly available on Zenodo: 3D outcrop model of Taşkent Şam Deresi (https://doi.org/10.5281/zenodo.16366010); 3D outcrop models of Çürük Dağ, Demirtaş, Öznurtepe, Taşkent Yolu (https://doi.org/10.5281/zenodo.16363427); Appendices 1–8 (https://doi.org/10.5281/zenodo.18886664).

ORCID

Baran Karapunar https://orcid.org/0000-0001-9711-1492
Stella Z. Buchwald https://orcid.org/0009-0004-3148-7226
Anja B. Frank https://orcid.org/0000-0001-8444-8440
Mónica Alejandra Gómez Correa https://orcid.org/0000-0003-2541-0551
Müjde Gürsoy https://orcid.org/0000-0002-6320-2000
Erdal Koşun https://orcid.org/0000-0002-8284-2118
Aymon Baud https://orcid.org/0000-0001-9799-6307
William J. Foster https://orcid.org/0000-0002-9595-8195

REFERENCES

Algeo, T.J. & Twitchett, R.J. (2010) Anomalous Early Triassic sediment fluxes due to elevated weathering rates and their biological consequences. *Geology*, 38, 1023–1026.

Aljinović, D. (1995) Storm influenced shelf sedimentation-an example from the Lower Triassic (Scythian) siliciclastic and carbonate succession near Knin (Southern Croatia and Western Bosnia and Herzegovina). *Geologia Croatica*, 48, 17–32.

Altıner, D. (1981) Recherches stratigraphiques et micropaléontologiques dans le Taurus Oriental au NW de Pinarbasi (Turquie), Faculté des sciences de l'Université de Genève, 1–450 pp.

Altıner, D., Özkan-Altıner, S., Atasoy, S.G. & Şahin, N. (2021) *Paynita permotaurica* n. gen., n. sp., and the other dagmaritin foraminifera from the Changhsingian (Permian) of southern Turkey: review of dagmaritin phylogeny. *Journal of Foraminiferal Research*, 51, 14–31.

Altıner, D., Özkan-Altıner, S. & Koçyiğit, A. (2000) Late Permian Foraminiferal Biofacies Belts in Turkey: palaeogeographic and Tectonic Implications. *Geological Society, London, Special Publications*, 173, 83–96.

Altıner, D., Payne, J.L., Lehrmann, D.J., Atasoy, S.G. & Özkan-Altıner, S. (2024) New foraminifera from the Changhsingian (Upper Permian) of the Taurides (southern Turkey) with remarks on their evolutionary origins. *Journal of Paleontology*, 98, 745–772.

Altıner, D. & Zaninetti, L. (1981) Le Trias dans la région de Pinarbasi, Taurus oriental, Turquie: Unités lithologiques, micropaléontologie, milieux de dépôt. *Rivista Italiana di Paleontologia*, 86, 705–760.

Angiolini, L., Carabelli, L., Nicora, A., Crasquin-Soleau, S., Marcoux, J. & Rettori, R. (2007) Brachiopods and other fossils from the Permo–Triassic boundary beds of the Antalya Nappes (SW Taurus, Turkey). *Geobios*, 40, 715–729.

Baud, A., Crasquin, S., Kershaw, S., Richoz, S., Kosun, E. & Forel, M. (2009) The Permian-Triassic transition in the Southwestern Taurus Mountains (South Turkey). In: *IGCP 572 annual Meeting & Field Workshop in southern Turkey, Antalya, Sept. 2-6, 2009*. Antalya: Akdeniz University, p. 47.

Baud, A., Magaritz, M. & Holser, W.T. (1989) Permian-Triassic of the Tethys: carbon isotope studies. *Geologische Rundschau*, 78, 649–677.

Baud, A., Richoz, S. & Marcoux, J. (2005) Calcimicrobial cap rocks from the basal Triassic units: western Taurus occurrences (SW Turkey). *Comptes Rendus Palevol*, 4, 569–582.

Beckert, J., Vandeginste, V. & John, C.M. (2016) Relationship between karstification and burial dolomitization in Permian platform carbonates (Lower Khuff—Oman). *Sedimentary Geology*, 342, 165–179.

Bittner, A. (1899) Versteinerungen aus den Trias- Ablagerungen des Süd – Ussuri – Gebietes in der ostsibirischen Küstenprovinz. *Mémories du comité Géologique*, 7(4), 1–35.

Bittner, A. (1901) Lamellibranchiaten aus der Trias des Bakonyer Waldes. *Resultate der wissenschaftlichen Erforschung des Balatonsees*, 2, 1–107.

Bozkaya, Ö. & Yalçın, H. (2005) Diagenesis and very low-grade metamorphism of the Antalya Unit: mineralogical evidence of Triassic rifting, Alanya-Gazipaşa, Central Taurus Belt, Turkey. *Journal of Asian Earth Sciences*, 25, 109–119.

Brandner, R., Horacek, M., Keim, L. & Scholger, R. (2009) The Pufels/Bulla road section: deciphering environmental changes across the Permian-Triassic boundary to the Olenekian by integrated litho-, magneto-and isotope stratigraphy. A field trip guide. *Geo. Alp*, 6, 116–132.

Broglio Loriga, C., Góczán, F., Haas, J., Lenner, K., Neri, C., Oravecz Sheffer, A., Posenato, R., Szabo, I. & Toth Makk, A. (1990) The Lower Triassic sequences of the Dolomites (Italy) and Transdanubian mid-mountains (Hungary) and their correlation. *Memorie di Scienze Geologiche, già Memorie degli Istituti di Geologia e Mineralogia dell'Università di Padova*, 42, 41–103.

Broglio Loriga, C., Masetti, D. & Neri, C. (1983) La Formazione di Werfen (Scitico) delle Dolomiti occidentali: sedimentologia e biostratigrafia. *Rivista Italiana di Paleontologia*, 88, 501–598.

Broglio Loriga, C. & Mirabella, S. (1986) Il genere *Eumorphotis* Bittner 1901 nella biostratigrafia dello Scitico, Formazione di Werfen (Dolomiti). *Memorie di Scienze Geologiche, già Memorie degli Istituti di Geologia e Mineralogia dell'Università di Padova*, 38, 245–281.

Broglio Loriga, C., Neri, C., Pasini, M. & Posenato, R. (1988) Marine fossil assemblages from Upper Permian to lowermost Triassic in the western Dolomites (Italy). *Memorie Della Società Geologica Italiana*, 34, 5–44.

Broglio Loriga, C. & Posenato, R. (1986) Costatoria (Costatoria?) subrotunda (Bittner, 1901). A Smithian (Lower Triassic) marker from Tethys. *Rivista Italiana di Paleontologia e Stratigrafia*, 92, 189–200.

Brönnimann, P., Zaninetti, L. & Bozorgnia, F. (1972) Triassic (Skythian) smaller foraminifera from the Elika Formation of the central Alborz, northern Iran, and from the Siusi Formation

20554877, 2026, 2, Downloaded from https://onlinelibrary.wiley.com/doi/10.1002/dep2.70071 by NICE, National Institute for Health and Care Excellence, Wiley Online Library on [14/04/2026]. See the Terms and Conditions (https://onlinelibrary.wiley.com/terms-and-conditions) on Wiley Online Library for rules of use; OA articles are governed by the applicable Creative Commons License

of the Dolomites, northern Italy. *Mitteilung Gesellschaft der Geologie-und Bergsbaustudenten, Innsbruck*, 21, 861–884.

Buchwald, S.Z., Birgel, D., Senger, K., Mosociova, T., Pei, Y., Frank, A.B., Galasso, F., Gómez Correa, M.A., Koşun, E., Karapunar, B., Wang, X., Kustatscher, E., Prinoth, H., Steinkrauss, R., Peckmann, J. & Foster, W.J. (2025) Primary productivity blooms on the Barents Shelf, Svalbard, associated with the 1 Permian Triassic mass extinction. *AGU Advances*, 6, e2025AV001785.

Crasquin-Soleau, S., Marcoux, J., Angiolini, L., Richoz, S., Nicora, A., Baud, A. & Bertho, Y. (2004) A new ostracode fauna from the Permian-Triassic boundary in Turkey (Taurus, Antalya Nappes). *Micropaleontology*, 50, 281–295.

Crasquin-Soleau, S., Richoz, S., Marcoux, J., Angiolini, L., Nicora, A. & Baud, A. (2002) Les événements de la limite Permien–Trias: derniers survivants et/ou premiers re-colonisateurs parmi les ostracodes du Taurus (Sud-Ouest de la Turquie). *Comptes Rendus Géoscience*, 334, 489–495.

Dai, J. & Zhang, J. (1989) Conodonts. In: Li, F. (Ed.) 2 (9)*Study of the Permo-Triassic Biostratigraphy and Event Stratigraphy of northern Sichuan and southern Shaanxi, Geological Memoir*. Beijing: Beijing Geological Publishing House, pp. 428–435.

Dal Corso, J., Song, H., Callegaro, S., Chu, D., Sun, Y., Hilton, J., Grasby, S.E., Joachimski, M.M. & Wignall, P.B. (2022) Environmental crises at the Permian–Triassic mass extinction. *Nature Reviews Earth & Environment*, 3, 197–214.

Demirtaşlı, E. (1967) *Lithostratigraphic units and petroleum prospects of the area between Pınarbaşı-Sarız-Mağara districts*, MTA Report No: 3489.

Emmrich, H. (1844) Über die Schichtenfolge der Flötz-Gebirge des Gader-Thales, der Seisser-Alpe und insbesondere bei St. Cassian. *Neues Jahrbuch für Mineralogie, Geologie und Paläontologie*, 1844, 791–803.

European Union. (2021) Regulation (EU) 2021/1119 of the European Parliament and of the Council of 30 June 2021 establishing the framework for achieving climate neutrality ('European Climate Law'). *Official Journal of the European Union*, 243, 1–17. Available from: http://data.europa.eu/eli/reg/2021/1119/oj

Farabegoli, E. & Perri, M.C. (2012) Millennial physical events and the end-Permian mass mortality in the western Palaeotethys: timing and primary causes. In: *Earth and life: global biodiversity, extinction intervals and biogeographic perturbations through time*. Dordrecht: Springer, pp. 719–758.

Farabegoli, E., Perri, M.C. & Posenato, R. (2007) Environmental and biotic changes across the Permian–Triassic boundary in western Tethys: the Bulla parastratotype, Italy. *Global and Planetary Change*, 55(1–3), 109–135.

Flügel, E. & Munnecke, A. (2010) *Microfacies of carbonate rocks: analysis, interpretation and application*. Berlin: Springer.

Forel, M.-B. (2015) Heterochronic growth of ostracods (Crustacea) from microbial deposits in the aftermath of the end-Permian extinction. *Journal of Systematic Palaeontology*, 13(4), 315–349.

Foster, W.J., Danise, S., Price, G.D. & Twitchett, R.J. (2018) Paleoecological analysis of benthic recovery after the late Permian mass extinction event in eastern Lombardy, Italy. *PALAIOS*, 33, 266–281.

Foster, W.J., Danise, S., Sedlacek, A., Price, G.D., Hips, K. & Twitchett, R.J. (2015) Environmental controls on the post-Permian recovery of benthic, tropical marine ecosystems in western Palaeotethys (Aggtelek Karst, Hungary). *Palaeogeography, Palaeoclimatology, Palaeoecology*, 440, 374–394.

Foster, W.J., Frank, A.B., Li, Q., Danise, S., Wang, X. & Peckmann, J. (2024) Thermal and nutrient stress drove Permian-Triassic shallow marine extinctions. *Cambridge Prisms: Extinction*, 2, 1–9.

Foster, W.J., Heindel, K., Richoz, S., Gliwa, J., Lehrmann, D.J., Baud, A., Kolar-Jurkovšek, T., Aljinović, D., Jurkovšek, B. & Korn, D. (2020) Suppressed competitive exclusion enabled the proliferation of Permian/Triassic boundary microbialites. *The Depositional Record*, 6(1), 62–74.

Foster, W.J., Lehrmann, D.J., Yu, M. & Martindale, R.C. (2019) Facies selectivity of benthic invertebrates in a Permian/Triassic boundary microbialite succession: implications for the "microbialite refuge" hypothesis. *Geobiology*, 17, 523–535.

Frank, A.B., Karapunar, B., Grasby, S.E., Koşun, E., Lahajnar, N., Gómez Correa, M.A., Buchwald, S.Z., Metzke, M. & Foster, W.J. (2025) Assessing the role of anoxia as a potential extinction driver in the shallow marine Neotethys during the Permian–Triassic mass extinction. *Chemical Geology*, 696, 123108.

Gliwa, J., Ghaderi, A., Leda, L., Schobben, M., Tomás, S., Foster, W.J., Forel, M.-B., Ghanizadeh Tabrizi, N., Grasby, S.E. & Struck, U. (2020) Aras Valley (northwest Iran): high-resolution stratigraphy of a continuous central Tethyan Permian–Triassic boundary section. *Fossil Record*, 23, 33–69.

Gliwa, J., Wiedenbeck, M., Schobben, M., Ullmann, C.V., Kiessling, W., Ghaderi, A., Struck, U. & Korn, D. (2022) Gradual warming prior to the end-Permian mass extinction. *Palaeontology*, 65(5), e12621.

Grant, R.E. (1968) Structural adaptation in two Permian brachiopod genera, Salt Range, West Pakistan. *Journal of Paleontology*, 42, 1–32.

Groves, J.R. & Altıner, D. (2005) Survival and recovery of calcareous foraminifera pursuant to the end-Permian mass extinction. *Comptes Rendus Palevol*, 4, 487–500.

Groves, J.R., Altıner, D. & Rettori, R. (2005) Extinction, survival, and recovery of lagenide foraminifers in the Permian–Triassic boundary interval, central Taurides, Turkey. *Journal of Paleontology*, 79, 1–38.

Güvenç, T. (1966) Description de quelques espèces d'algues calcaires (Gymnocodiacées et Dasycladacées) du Carbonifère et du Permien des Taurus Occidentaux. *Revue de Micropaleontologie*, 9(2), 94–103.

Haas, J., Demény, A., Hips, K., Zajzon, N., Weiszburg, T.G., Sudar, M. & Pálfy, J. (2007) Biotic and environmental changes in the Permian–Triassic boundary interval recorded on a western Tethyan ramp in the Bükk Mountains, Hungary. *Global and Planetary Change*, 55, 136–154.

Hauer, F.v. (1850) Ueber die von Herrn Bergrath W. Fuchs in den Venetianer Alpen gesammelten Fossilien. *Denkschriften der Kaiserlichen Akademie der Wissenschaften/Mathematisch-Naturwissenschaftliche Classe*, 2, 109–126.

Heindel, K., Foster, W.J., Richoz, S., Birgel, D., Roden, V.J., Baud, A., Brandner, R., Krystyn, L., Mohtat, T. & Koşun, E. (2018) The formation of microbial-metazoan bioherms and biostromes following the latest Permian mass extinction. *Gondwana Research*, 61, 187–202.

Herminghaus, S., Thomas, K.R., Aliaskarisohi, S., Porada, H. & Goehring, L. (2016) Kinneyia: a flow-induced anisotropic fossil

20554877, 2026, 2, Downloaded from https://onlinelibrary.wiley.com/doi/10.1002/dep2.70071 by NICE, National Institute for Health and Care Excellence, Wiley Online Library on [14/04/2026]. See the Terms and Conditions (https://onlinelibrary.wiley.com/terms-and-conditions) on Wiley Online Library for rules of use; OA articles are governed by the applicable Creative Commons License

pattern from ancient microbial mats. *Frontiers in Materials*, 3, 30.

Hips, K. (1998) Lower Triassic storm-dominated ramp sequence in northern Hungary: an example of evolution from homoclinal through distally steepened ramp to Middle Triassic flat-topped platform. *Geological Society, London, Special Publications*, 149, 315–338.

Hofmann, R., Hautmann, M. & Bucher, H. (2015) Recovery dynamics of benthic marine communities from the Lower Triassic Werfen Formation, northern Italy. *Lethaia*, 48, 474–496.

Jurikova, H., Gutjahr, M., Wallmann, K., Flögel, S., Liebetrau, V., Posenato, R., Angiolini, L., Garbelli, C., Brand, U. & Wiedenbeck, M. (2020) Permian–Triassic mass extinction pulses driven by major marine carbon cycle perturbations. *Nature Geoscience*, 13(11), 745–750.

Kahsnitz, M.M. & Willems, H. (2019) Genesis of Paleocene and Lower Eocene shallow-water nodular limestone of South Tibet (China). *Carbonates and Evaporites*, 34, 199–218.

Kalafatçıoğlu, A. (1973) Geology of the western part of Antalya Bay. *Bulletin of the Mineral Research and Exploration*, 81, 31–84.

Kershaw, S., Crasquin, S., Forel, M.B., Randon, C., Collin, P.Y., Kosun, E., Richoz, S. & Baud, A. (2011) Earliest Triassic microbialites in Çürük Dag, southern Turkey: composition, sequences and controls on formation. *Sedimentology*, 58, 739–755.

Kershaw, S., Crasquin, S., Li, Y., Collin, P.Y., Forel, M.B., Mu, X., Baud, A., Wang, Y., Xie, S. & Maurer, F. (2012) Microbialites and global environmental change across the Permian–Triassic boundary: a synthesis. *Geobiology*, 10, 25–47.

Korte, C. & Kozur, H.W. (2010) Carbon-isotope stratigraphy across the Permian–Triassic boundary: a review. *Journal of Asian Earth Sciences*, 39, 215–235.

Kozur, H. & Pjatakova, M. (1976) Die Conodontenart *Anchignathodus parvus* n. sp., eine wichtige Leitform der basalen Trias von Nord- und Zentral-Iran. *Koninklijke Nederlandse Akademie Van Wetenschappen-Amsterdam, Reprinted from Proceedings, Series B*, 79, 123–128.

Kozur, H.W. (1996) The conodonts *Hindeodus*, *Isarcicella* and *Sweetohindeodus* in the uppermost Permian and lowermost Triassic. *Geologia Croatica*, 49, 81–115.

Kozur, H.W., Kaya, O. & Mostler, H. (1996) First evidence of Lower to middle Scythian (Dienerian-lower Olenekian) radiolarians from the Karakaya Zone of northwestern Turkey. *Geologisch-Palaontologische Mitteilungen Innsbruck, Sonderband*, 4, 271–285.

Kraus, S.H., Siegert, S., Mette, W., Struck, U. & Korte, C. (2009) Stratigraphic significance of carbon isotope variations in the shallow-marine Seis/Siusi Permian–Triassic boundary section (Southern Alps, Italy). *Fossil Record*, 12, 197–205.

Lau, K.V., Maher, K., Altıner, D., Kelley, B.M., Kump, L.R., Lehrmann, D.J., Silva-Tamayo, J.C., Weaver, K.L., Yu, M. & Payne, J.L. (2016) Marine anoxia and delayed Earth system recovery after the end-Permian extinction. *Proceedings of the National Academy of Sciences*, 113(9), 2360–2365.

Lehrmann, D.J., Payne, J.L., Felix, S.V., Dillett, P.M., Wang, H., Yu, Y. & Wei, J. (2003) Permian–Triassic boundary sections from shallow-marine carbonate platforms of the Nanpanjiang Basin, South China: implications for oceanic conditions associated with the end-Permian extinction and its aftermath. *PALAIOS*, 18, 138–152.

Leighton, L.R. (2000) Environmental distribution of spinose brachiopods from the Devonian of New York: test of the soft-substrate hypothesis. *PALAIOS*, 15, 184–193.

Lerosey-Aubril, R. & Angiolini, L. (2009) Permian trilobites from Antalya Province, Turkey, and enrollment in Late Palaeozoic trilobites. *Turkish Journal of Earth Sciences*, 18, 427–448.

Li, F., Yan, J., Chen, Z.-Q., Ogg, J.G., Tian, L., Korngreen, D., Liu, K., Ma, Z. & Woods, A.D. (2015) Global oolite deposits across the Permian–Triassic boundary: a synthesis and implications for palaeoceanography immediately after the end-Permian biocrisis. *Earth-Science Reviews*, 149, 163–180.

Loope, G.R., Kump, L.R. & Arthur, M.A. (2013) Shallow water redox conditions from the Permian–Triassic boundary microbialite: the rare earth element and iodine geochemistry of carbonates from Turkey and South China. *Chemical Geology*, 351, 195–208.

Lys, M. & Marcoux, J. (1978) Les niveaux du Permien supérieur des Nappes d'Antalya (Taurides occidentales, Turquie). *Compte Rendu Hebdomadaire des Séances de l'Académie des Sciences, Paris, Série D*, 286, 1417–1420.

Marcoux, J. & Baud, A. (1988) The Permo-Triassic boundary in the Antalya Nappes (Western Taurides-Turkey). *Memorie della Società Geologica Italiana, IGCP Project 203 Special Volume*, 34, 243–252.

Marcoux, J., Baud, A., Krystyn, L. & Monod, O. (1986) Guide book part 2, Western Taurides, Antalya – Seydisehir – Isparta – Antalya. In: Marcoux, J. (Ed.) *Late Permian and Triassic in Western Turkey, Field Workshop 1986*, Vol. 2. Istanbul: Istanbul Technical University, pp. 1–64.

Marshall, C.R. (2023) Forty years later: the status of the "Big Five" mass extinctions. *Cambridge Prisms: Extinction*, 1, e5.

Mata, S. & Bottjer, D. (2012) Microbes and mass extinctions: paleoenvironmental distribution of microbialites during times of biotic crisis. *Geobiology*, 10(1), 3–24.

Münster, G.z. (1841) Beschreibung und Abbildung der in den Kalkmergelschichten von St. Cassian gefundenen Versteinerungen. In: Wissmann, H.L., Münster, G.z. & Braun, K.F. (Eds.) *Beiträge zur Geologie und Petrefacten-Kunde des südöstlichen Tirol's vorzüglich der Schichten von St. Cassian*. Bayreuth: Buchner, pp. 25–152.

Neri, C. & Posenato, R. (1985) New biostratigraphical data on uppermost Werfen Formation of western Dolomites (Trento Italy). *Geologische und Paläontologische Mitteilungen Innsbruck*, 14, 87–107.

Özgül, N. (1984) Stratigraphy and tectonic evolution of the Central Taurides. In: *Geology of the Taurus Belt. International Symposium*. Ankara: Geological Society of Turkey and the Mineral Research and Exploration Institute, pp. 77–90.

Özgül, N. (1985) Alanya Tectonic window and geology of its western part. In: *Ketin Symposium*. Ankara: Türkiye Jeoloji Kurumu, pp. 97–120.

Özgül, N. (1997) Stratigraphy of the tectonostratigraphic units around Bozkır-Hadim-Taşkent region (northern part of the Central Taurides). *Bulletin of the Mineral Research and Exploration*, 119, 113–174.

Özgül, N., Metin, S., Göğer, E., Bingöl, İ., Baydar, O. & Erdoğan, B. (1973) Tufanbeyli dolayının (Doğu Toroslar, Adana) Kambriyen-Tersiyer kayaları. *Türkiye Jeoloji Kurumu Bülteni*, 16, 82–100.

Payne, J.L., Lehrmann, D.J., Follett, D., Seibel, M., Kump, L.R., Riccardi, A., Altıner, D., Sano, H. & Wei, J. (2007) Erosional

20554877, 2026, 2, Downloaded from https://onlinelibrary.wiley.com/doi/10.1002/dep2.70071 by NICE, National Institute for Health and Care Excellence, Wiley Online Library on [14/04/2026]. See the Terms and Conditions (https://onlinelibrary.wiley.com/terms-and-conditions) on Wiley Online Library for rules of use; OA articles are governed by the applicable Creative Commons License

truncation of uppermost Permian shallow-marine carbonates and implications for Permian-Triassic boundary events. *Geological Society of America Bulletin*, 119, 771–784.
Posenato, R. (2008) Global correlations of mid Early Triassic events: the Induan/Olenekian boundary in the Dolomites (Italy). *Earth-Science Reviews*, 91, 93–105.
Posenato, R. (2019) The end-Permian mass extinction (EPME) and the Early Triassic biotic recovery in the western Dolomites (Italy): state of the art. *Bollettino della Societa Paleontologica Italiana*, 58, 11–34.
Pratt, B.R. (2021) Kinneyia-type wrinkle structures on sandstone beds: not microbially induced but deformation features caused by synsedimentary earthquakes. *PALAIOS*, 36, 313–325.
Pruss, S., Fraiser, M. & Bottjer, D.J. (2004) Proliferation of Early Triassic wrinkle structures: implications for environmental stress following the end-Permian mass extinction. *Geology*, 32, 461–464.
Pruss, S.B., Bottjer, D.J., Corsetti, F.A. & Baud, A. (2006) A global marine sedimentary response to the end-Permian mass extinction: examples from southern Turkey and the western United States. *Earth-Science Reviews*, 78, 193–206.
Quenstedt, F.A. (1849) *Petrefactenkunde Deutschlands, Cephalopoden*. Tübingen: LF Fues.
Riccardi, A. (2007) *Carbonate-associated sulfate: assessment of and use as an isotopic proxy for global sulfur cycling during end-permian mass extinction*. Pennsylvania: The Pennsylvania State University.
Richoz, S. (2006) Stratigraphie et variations isotopiques du carbone dans le Permien supérieur et le Trias inférieur de quelques localités de la Néotéthys (Turquie, Oman et Iran). *Mémoires de Géologie (Lausanne)*, 46, 1–251.
Robertson, A.H., Parlak, O. & Ustaömer, T. (2012) Overview of the Palaeozoic–Neogene evolution of neotethys in the Eastern Mediterranean region (southern Turkey, Cyprus, Syria). *Petroleum Geoscience*, 18, 381–404.
Robertson, A.H., Ustaömer, T., Pickett, E.A., Collins, A.S., Andrew, T. & Dixon, J.E. (2004) Testing models of Late Palaeozoic–Early Mesozoic orogeny in Western Turkey: support for an evolving open-Tethys model. *Journal of the Geological Society*, 161, 501–511.
Rogov, M., Ershova, V., Gaina, C., Vereshchagin, O., Vasileva, K., Mikhailova, K. & Krylov, A. (2023) Glendonites throughout the Phanerozoic. *Earth-Science Reviews*, 241, 104430.
Şahin, N. & Altıner, D. (2019) Testing of Permian–Lower Triassic stratigraphic data in a half-graben/tilt-block system: evidence for the initial rifting phase in Antalya Nappes. *Canadian Journal of Earth Sciences*, 56, 1262–1283.
Schubert, J.K. & Bottjer, D.J. (1992) Early Triassic stromatolites as post-mass extinction disaster forms. *Geology*, 20(10), 883–886.
Şenel, M. (1997) *1:100,000 scale Türkiye Geological Maps, No. 7, Antalya O24 Sheet*. Ankara: MTA General Directorate Geological Surveys Department.
Şenel, M., Bedi, M. & Çörekcioğlu, E. (2016) *1:100,000 scale Türkiye Geological Maps, No. 7, Antalya O24 Sheet*. Ankara: MTA General Directorate Geological Surveys Department.
Senger, K., Betlem, P., Birchall, T., Gonzaga, L., Jr., Grundvåg, S.-A., Horota, R.K., Laake, A., Kuckero, L., Mørk, A. & Planke, S. (2022) Digitising Svalbard's geology: the Festningen digital outcrop model. *First Break*, 40, 47–55.
Şengör, A.M.C. & Yılmaz, Y. (1981) Tethyan evolution of Turkey: a plate tectonic approach. *Tectonophysics*, 75, 181–241.
Shen, S.-Z., Crowley, J.L., Wang, Y., Bowring, S.A., Erwin, D.H., Sadler, P.M., Cao, C.-q., Rothman, D.H., Henderson, C.M. & Ramezani, J. (2011) Calibrating the end-Permian mass extinction. *Science*, 334, 1367–1372.
Sperling, E.A., Boag, T.H., Duncan, M.I., Endriga, C.R., Marquez, J.A., Mills, D.B., Monarrez, P.M., Sclafani, J.A., Stockey, R.G. & Payne, J.L. (2022) Breathless through time: oxygen and animals across Earth's history. *The Biological Bulletin*, 243(2), 184–206.
Stache, G. (1878) Beiträge zur Fauna der Bellerophonkalke Südtirols. Nr. 2. Pelecypoden und Brachiopoden. *Jahrbuch der kaiserlich-königlichen geologischen Reichsanstalt*, 28(Heft 1), 93–168.
Stampfli, G., Marcoux, J. & Baud, A. (1991) Tethyan margins in space and time. *Palaeogeography, Palaeoclimatology, Palaeoecology*, 87, 373–409.
Török, Á. (1998) Controls on development of Mid-Triassic ramps: examples from southern Hungary. *Geological Society, London, Special Publications*, 149, 339–367.
Twitchett, R.J. & Wignall, P.B. (1996) Trace fossils and the aftermath of the Permo-Triassic mass extinction: evidence from northern Italy. *Palaeogeography, Palaeoclimatology, Palaeoecology*, 124, 137–151.
Ünal, E., Altıner, D., Yılmaz, I.Ö. & Özkan-Altıner, S. (2003) Cyclic sedimentation across the Permian–Triassic boundary (central Taurides, Turkey). *Rivista Italiana di Paleontologia e Stratigrafia*, 109, 359–376.
Varol, B., Koşun, E., Pinar, N.Ü. & Ayranci, K. (2011) Pyritized mudstone and associated facies in the Permian–Triassic boundary of the Çürük Dağ section, Southern Turkey. *Journal of Asian Earth Sciences*, 40, 1068–1078.
Verna, V., Angiolini, L., Baud, A., Crasquin, S. & Nicora, A. (2011) Guadalupian brachiopods from western Taurus, Turkey. *Rivista Italiana di Paleontologia e Stratigrafia*, 117, 51–104.
von Richthofen, F.F. (1860) *Geognostische Beschreibung der Umgegend von Predazzo, Sanct Cassian und der Seisser Alpe in Süd-Tyrol*. Gotha: Justus Perthes.
Wang, X., Zhong, H., Chen, J., Lin, Z., Wang, B., Hou, M., Li, Y. & Wang, C. (2024) DDE-Outcrop3D: a new pathway to the Deep-time Earth, EGU General Assembly 2024, Vienna, Austria, 14–19 Apr 2024, EGU24-16328. https://doi.org/10.5194/egusphere-egu24-16328
Wang, Y., Sadler, P.M., Shen, S.-z., Erwin, D.H., Zhang, Y.-c., Wang, X.-d., Wang, W., Crowley, J.L. & Henderson, C.M. (2014) Quantifying the process and abruptness of the end-Permian mass extinction. *Paleobiology*, 40(1), 113–129.
Wignall, P.B. & Twittchett, R.J. (1999) Unusual intraclastic limestones in Lower Triassic carbonates and their bearing on the aftermath of the end-Permian mass extinction. *Sedimentology*, 46, 303–316.
Wilkinson, M.D., Dumontier, M., Aalbersberg, I.J., Appleton, G., Axton, M., Baak, A., Blomberg, N., Boiten, J.-W., da Silva Santos, L.B. & Bourne, P.E. (2016) The FAIR Guiding Principles for scientific data management and stewardship. *Scientific Data*, 3, 160018.
Xu, Z., Yu, J., Yin, H., Merdith, A.S., Hilton, J., Allen, B.J., Gurung, K., Wignall, P.B., Dunhill, A.M. & Shen, J. (2025) Early Triassic super-greenhouse climate driven by vegetation collapse. *Nature Communications*, 16, 5400.

20554877, 2026, 2, Downloaded from https://onlinelibrary.wiley.com/doi/10.1002/dep2.70071 by NICE, National Institute for Health and Care Excellence, Wiley Online Library on [14/04/2026]. See the Terms and Conditions (https://onlinelibrary.wiley.com/terms-and-conditions) on Wiley Online Library for rules of use; OA articles are governed by the applicable Creative Commons License

Yan, J. & Carlson, E.H. (2003) Nodular celestite in the Chihsia formation (Middle Permian) of south China. *Sedimentology*, 50(2), 265–278.

Yin, H.-F., Zhang, K., Tong, J., Yang, Z. & Wu, S. (2001) The global stratotype section and Point (GSSP) of the Permian-Triassic boundary. *Episodes*, 24, 102–114.

Zhang, H., Zhang, F., Chen, J.-b., Erwin, D.H., Syverson, D.D., Ni, P., Rampino, M., Chi, Z., Cai, Y.-f. & Xiang, L. (2021) Felsic volcanism as a factor driving the end-Permian mass extinction. *Science Advances*, 7(47), eabh1390.

SUPPORTING INFORMATION

Additional supporting information can be found online in the Supporting Information section at the end of this article.

How to cite this article: Karapunar, B., Wang, X., Buchwald, S.Z., Frank, A.B., Gómez Correa, M.A., Gürsoy, M. et al. (2026) The Permian–Triassic transition in Türkiye: New insights and 3D outcrop models for accessible, reproducible and sustainable fieldwork. *The Depositional Record*, 12, e70071. Available from: https://doi.org/10.1002/dep2.70071

20554877, 2026, 2, Downloaded from https://onlinelibrary.wiley.com/doi/10.1002/dep2.70071 by NICE, National Institute for Health and Care Excellence, Wiley Online Library on [14/04/2026]. See the Terms and Conditions (https://onlinelibrary.wiley.com/terms-and-conditions) on Wiley Online Library for rules of use; OA articles are governed by the applicable Creative Commons License